A THREE-POLE ANALOG CANCELLATION FILTER WITH VARIABLE PASSBAND FOR USE IN RANGE-GATED RADARS

by

Harold Lee Broberg

United States Naval Postgraduate School

THESIS

A THREE-POLE ANALOG CANCELLATION FILTER WITH VARIABLE PASSBAND FOR USE IN RANGE-GATED RADARS

by

Harold Lee Broberg

December 1969

This document has been approved for public release and sale; its distribution is unlimited.

A Three-Pole Analog Cancellation Filter with Variable Passband for use in Range-Gated Radars

by

Harold Lee Broberg
Captain, United States Marine Corps
B.A., Northwestern University, 1963

Submitted in partial fulfillment of the
requirements for the degree of

MASTER OF SCIENCE IN ELECTRICAL ENGINEERING

from the

NAVAL POSTGRADUATE SCHOOL
December 1969

ABSTRACT

The design considerations and synthesis procedures involved in construction of a variable-passband analog cancellation filter for use in a range-gated Moving-Target-Indicator (MTI) radar are presented. A three-pole Chebychev comb filter built using field-effect transistors and integrated-circuit operational amplifiers was tested and the results are compared with theoretical values. The merits of this type of filter in a range-gated radar are discussed and the performance of a complete range channel containing the filter is compared in the AN/UPS-1 air-search radar with normal radar operation using a delay-line canceller.

TABLE OF CONTENTS

LIST OF TABLES

LIST OF FIGURES

I. INTRODUCTION

The performance of a modern surveillance radar must meet many demanding specifications. Several factors which must be considered are the wide range of aircraft speeds (from helicopters to supersonic jets) and the large amount of air traffic. In the case of military radars, the increased ability of an enemy to utilize active and passive countermeasures to decrease the detection capabilities of the radar must also be taken into account. Many times it is necessary to try a new approach to solve the problems presented by more stringent performance criterion. This is the case in dealing with the requirement for an MTI radar to have an increased subclutter visibility[1] without increasing the signal-to-noise ratio required to detect a target in the clear.

A. DELAY-LINE CANCELLERS

The delay-line canceller MTI radar uses the change in frequency of the radar return signal from a moving target to distinguish it from fixed targets. This frequency change is due to the well known Doppler shift of a moving object. The relationship

---

[1] Subclutter visibility is the maximum ratio of the echo power received from a stationary object to the power received back from a moving target for which the target can still be observed using the Doppler effect and is usually expressed in decibels (dB).

between Doppler frequency and the velocity of a target is given by:

$$F_d = \frac{2V_r}{\lambda}$$

V_r = radial component of target velocity

λ = wavelength of radar

F_d = Doppler frequency

Successive radar pulses returned from a moving target are, after detection in a phase-sensitive detector, amplitude modulated at the Doppler frequency of the target. Successive pulse returns from a stationary target, however, have the same amplitude. Since pulses are separated in time by the pulse-repetition period of the radar, if successive pulses are subtracted the stationary targets are eliminated and only moving targets remain. This subtraction (cancellation) is done by providing two signal paths for the pulse return (after mixing down to video frequency), one straight thru path and one path introducing a delay equal to the pulse-repetition period. A block diagram of a typical delay-line cancellation unit is shown in Figure 1(a) without the timing and automatic gain control (AGC) circuitry. A more complete discussion of delay lines and cancellers is given in Ref. 1.

Radars using delay-line cancellers are the earliest form of MTI radars and are still the principal type employed. The sub-clutter visibility and required signal-to-noise ratio of this type of radar has been improved along with normal improvements in the components of the system, but a number of deficiencies still exist

(a) Block Diagram

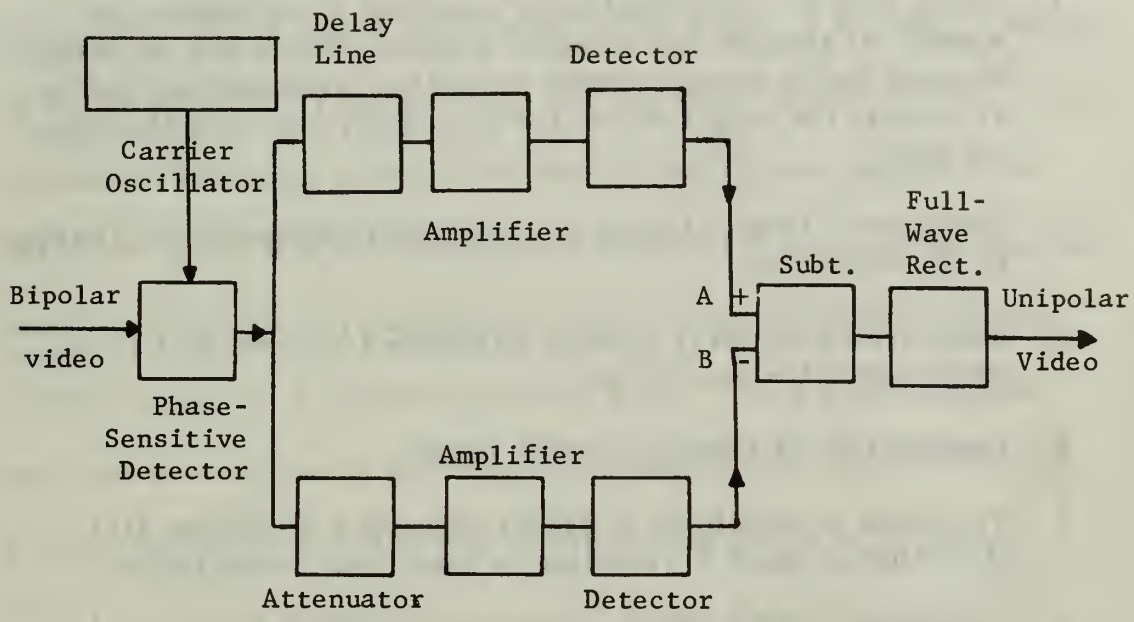

(b) Frequency Response

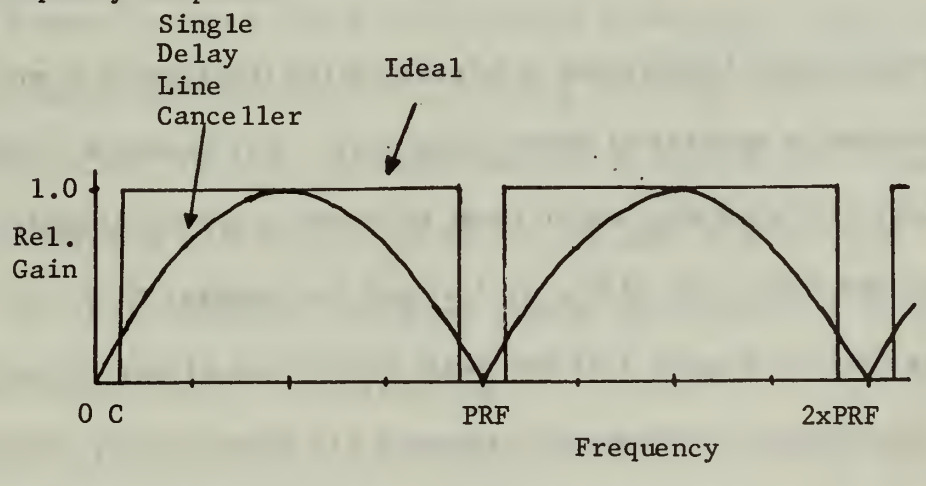

FIGURE 1: SINGLE DELAY-LINE CANCELLER

which limit the performance of the delay-line canceller. Some of the main drawbacks of the delay-line canceller are listed below.

1. Large loss due to transducers required to transform the electrical signals into acoustic signals, which can be readily delayed due to a much lower velocity of propagation, and to reconvert the output of the acoustic delay line into electrical signals.

2. Instability of exact length of delay due to temperature changes in the delay line.

3. Undesired secondary signals introduced by unwanted reflections within the delay line.

4. Degradation of signal-to-noise ratio.

5. Variation in amplitude of signal at point A of Figure 1(a) from that at point B resulting in imperfect cancellation.

6. Breakdown of a single key component renders the entire system inoperable.

7. Inefficient Doppler filter characteristics of a single delay-line canceller as shown in Figure 1(b).

Some fundamental limitations in present delay lines prevent much improvement in several of these categories. For instance, transducer loss (40 to 60 db), which must be made up by the amplifier following the delay line of Figure 1(a) and the Doppler filter characteristic of Figure 1(b) are basic properties of this method. More ideal Doppler-frequency responses are theoretically possible using several delay lines and feedback, but because of the cost of present delay lines, a multiplicity of extremely tight tolerances, and stability problems with the feedback loop this has not proven to be feasible.

B. RANGE GATING

An MTI radar can also be constructed using range-gated filtering (RGF) in which the bipolar video output is fed into a series of range channels, each of which represents a range interval comparable to the pulse width of the radar. Successive pulses from the same target are therefore processed by the same range channel and the elimination of stationary targets is accomplished in each channel by use of a clutter-rejection filter. This eliminates the need for a delay line in the video-processing unit of an MTI radar. A more complete presentation of range-gated radars is given in Ref. 1. A block diagram of a typical range channel is shown in Figure 2(a).

The principles and theory involved in MTI by RGF have been well known for many years, but because of the size, weight and cost considerations involved in building the large number of channels required, this type of radar was not practical until recently. As an example of the large number of circuits involved, the AN/UPS-1 (a delay-line canceller type of radar) has a 1.4-microsecond pulse width, corresponding to a range interval of 420 meters; an MTI by RGF radar having the same gate width and a range of 80 nautical miles would require 715 channels.

The MTI by RGF concept theoretically removes most of the deficiencies in a delay-line canceller MTI. For instance, all

(a) Block Diagram of a Single Range Channel

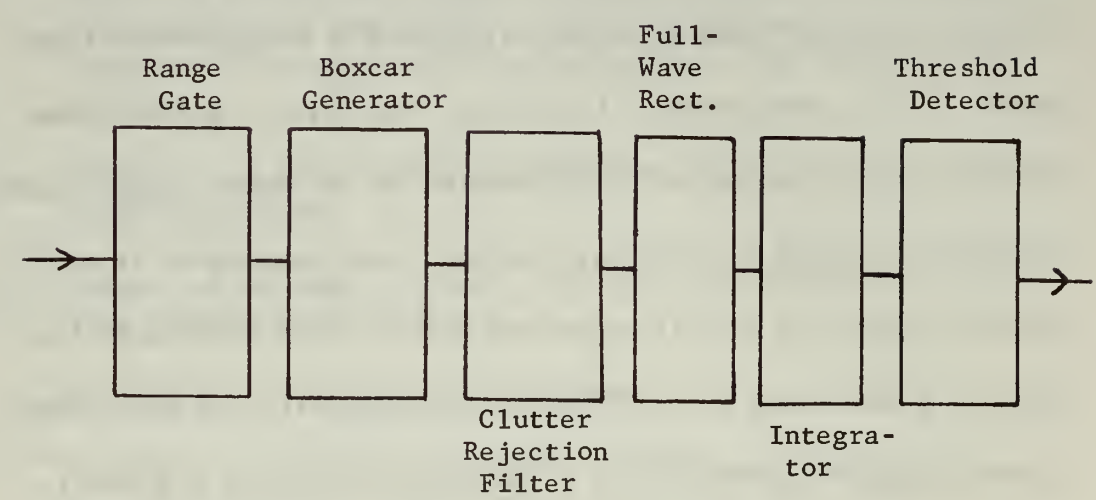

(b) Frequency Response

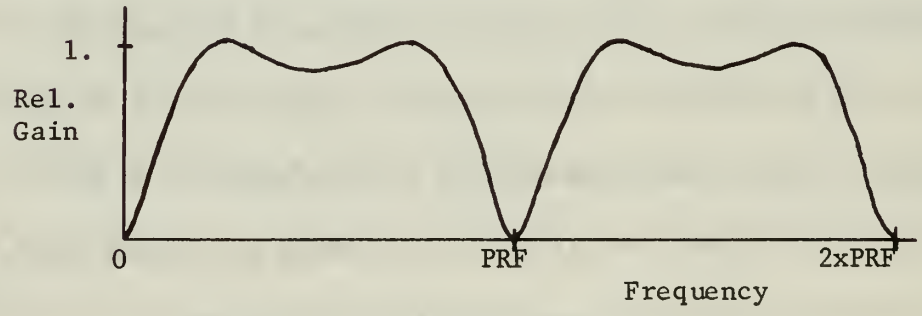

FIGURE 2: MTI BY RGF

channels are operated in parallel so that if one breaks down very little information is lost. Also, improvement in the Doppler filter characteristic can be accomplished thru use of more ideal filters. A two-pole filter characteristic is shown in Figure 2(b) corresponding to the response of an RGF video processor which has been built and is discussed in Ref. 2. The response of this filter is much closer to the ideal characteristic than is the response of the delay-line canceller shown in Figure 1(b).

The advent of integrated circuits and large-scale-integration (LSI) has made the construction of hundreds of circuits in a small package possible. This has allowed the practical implementation of range-gated radars with the result that increased subclutter visibility and better signal-to-noise ratio have been obtained than was possible with delay-line cancellers.

Perhaps the most important part of a range channel is the filter since its characteristic determines the Doppler-frequency response of the entire system. A desirable feature of this filter, in addition to a flat passband, is a variable rejection bandwidth to permit adaption to different clutter spectral characteristics.

Construction of the filter can be accomplished using any of four general types of filters which are listed below.

1. L-C bandpass filter
2. Active bandpass filter
3. Digital filter

4. Active analog cancellation filter

Since the filter is designed for use in the low-frequency range (for a radar with a pulse-repetition frequency (PRF) of 800 hertz (Hz) the passband would have a lower cutoff frequency of about 20 Hz) an L-C filter is impractical in terms of the size of the elements required.

Active bandpass filters using Operational Amplifiers (OPAMPS) for use in range-gated radars are considered in Ref. 3, and two operational MTI by RGF systems using active filters in the range channels are discussed in Refs. 2 and 4.

Digital MTI filters are discussed in Ref. 5 and do not strictly fit into the block diagram of Figure 2(a). They are basically range-gated and have been included here because of the importance of the concept of digital filtering in radar processing. In addition, the process of weighted pulse cancellation of range-gated pulses used in digital form can be similarly implemented in analog form as a method of synthesis of the analog cancellation filter.

The active analog cancellation filter utilizes the same principles involved in a delay-line canceller except that the filter must only cancel stationary target returns received from a single range interval. The frequency response of the analog filter is thus periodic at the PRF of the radar.

The remainder of this paper develops synthesis and construction techniques for variable-passband analog cancellation

filters, and discusses the building and testing of such a filter and its associated range channel.

II. FILTER DESIGN

The design of the filter must take a number of factors into account such as the method of cancellation to be used, the desired frequency response, the number of components required and the method of synthesis to be used. The final design must be the result of a trade-off between how closely the response approaches optimum and the maximum number of components considered practical.

A. DESIRED FILTER CHARACTERISTICS

The ideal filter characteristic shown in Figure 1(b) does not indicate the frequency of the point marked C below which there is infinite attenuation and which determines the width of the stop-band at multiples of the PRF. If all clutter were stationary with respect to the antenna, such as a tower being irradiated by radar pulses from a motionless antenna, this clutter-rejection notch would only have to reject signals at zero frequency. This is obviously not the case since surveillance radars must have scanning antennas, and clutter can have widely varying velocities (Doppler frequencies) depending on a number of variables. Some of the factors influencing the maximum Doppler frequency of clutter in addition to the radar carrier frequency are: variable weather conditions (clouds, precipitation, sea state), geography of the area surrounding the radar site and presence of passive radar countermeasures such as chaff. An example of the Doppler-frequency range of various types

(a) Clutter Frequencies

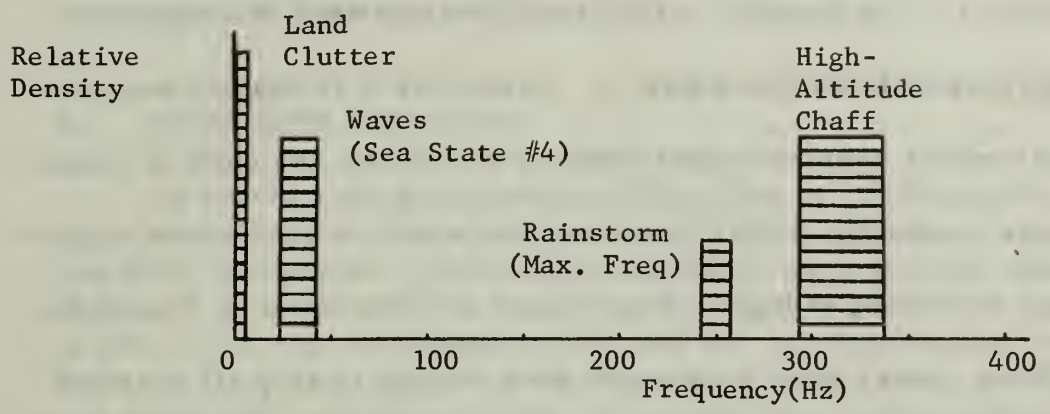

(b) Ideal Filter with Broad Passband

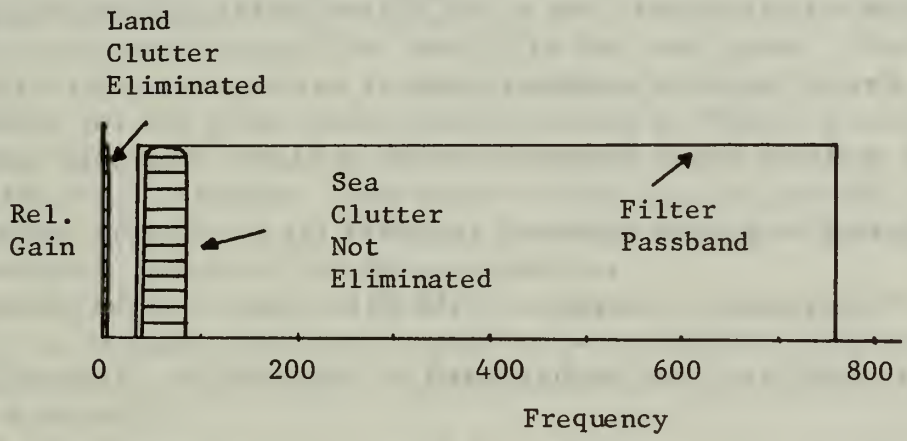

(c) Ideal Filter with Narrow Passband

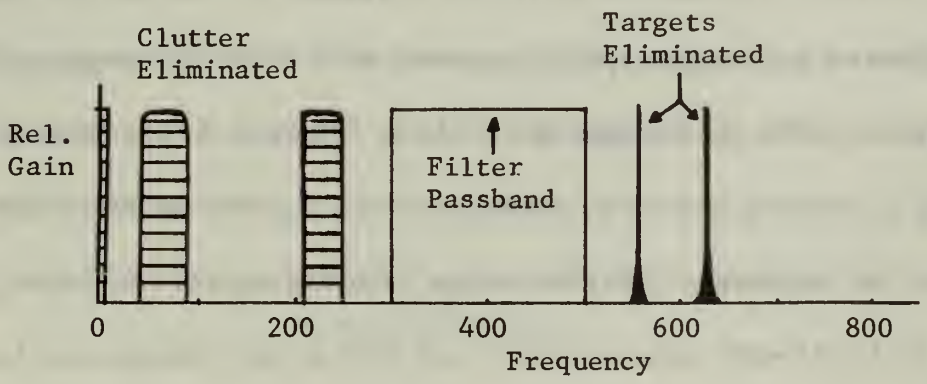

FIGURE 3: ILLUSTRATION OF CLUTTER EFFECTS

of clutter is shown in Figure 3(a) for an L-band radar such as the AN/UPS-1. The Doppler velocity information used to construct this Figure is taken from Ref. 6. From this it is readily seen that a filter with a constant cutoff frequency could be designed to counter a single maximum clutter frequency but would be ineffective against clutter occurring at higher frequencies as illustrated in Figure 3(b) and if the clutter band were made wide enough to stop all possible natural clutter as shown in Figure 3(c) not many moving targets would be visible either, due to the narrow passband remaining.

From the above considerations it was apparent that a filter with a variable cutoff frequency would be highly desirable and could be adjusted to give an optimum response for any clutter conditions.

The frequency response of the delay line or of the analog cancellation filter can be discussed in normal filter terminology by considering the response only from zero frequency to the PRF of the radar. Using this basis the response of Figure 1(b) can be considered as a single-pole response with all of the response characteristics of a single-pole filter. Thus in order to design the filter a decision had to be made as to the number of poles and hence the number of dB-per-octave falloff desired. A 3-pole filter has an 18-dB-per-octave falloff and with proper design can be made to have a good passband shape. The type of filter characteristic to be used was selected using standard filter design techniques. The Chebychev 3-pole filter was chosen from among the standard

filter types (Butterworth, elliptic, Chebychev, etc.) and has a characteristic shown in Ref. 1 and 7.

B. SYNTHESIS METHODS

An active analog cancellation filter can be synthesized using two basic techniques. One can be thought of as a parallel operation in which successive pulses are delayed for varying lengths of time and added with weighting factors to produce the desired characteristic. Figure 4(a) illustrates a system in which five successive pulses are added to yield the best fit to the ideal case. The frequency response for the given coefficients is shown in Figure 4(b) along with the ideal response. The output of the filter is just the sum of the delayed inputs and can be expressed as:

$$V_o = a_o + a_1 \exp(-j\omega T) + a_2 \exp(-j2\omega T) + a_3 \exp(-j3\omega T) + a_4 \exp(-j4\omega T)$$

where the term:

$\exp(j\omega T)$ (in which ω = frequency in radians)

is the transfer function of a delay of time T and in this case T would represent a multiple of 1/PRF of the radar. This expression can be rewritten as:

$$V_o = \exp(-j2\omega T)[\, a_o \exp(j2\omega T) + a_1 \exp(j\omega T) + a_2 + a_3 \exp(-j\omega T) + a_4 \exp(-j2\omega T)\,]$$

If the phase term is neglected the expression can be seen to resemble the first few terms of a complex Fourier series. The coefficients can be computed from the Fourier series for the ideal

(a) 5-Pulse Cancellation

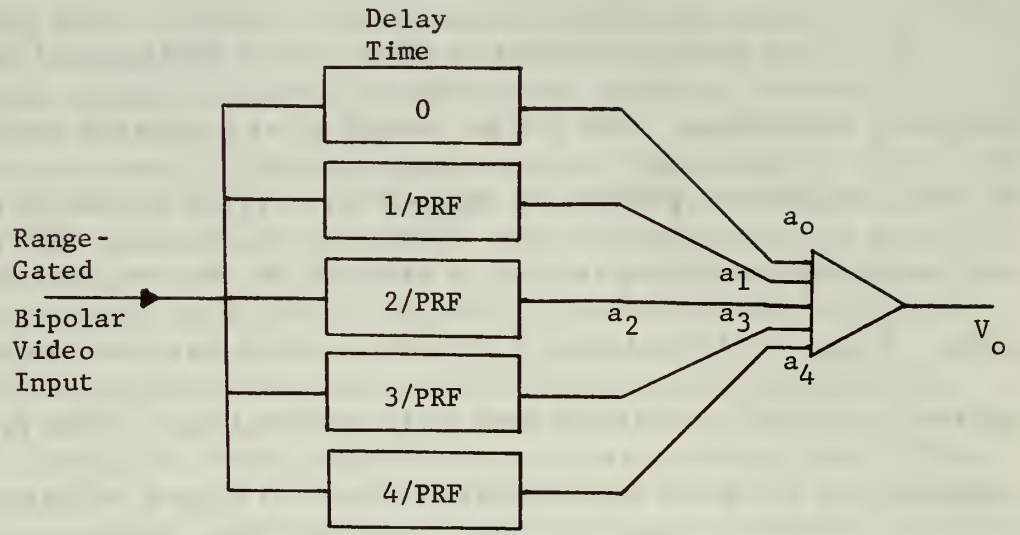

(b) Frequency response of (a) with: $a_0 = -.866$, $a_1 = -1.$
$a_2 = 3.73$, $a_3 = -1.$
$a_4 = -.866$

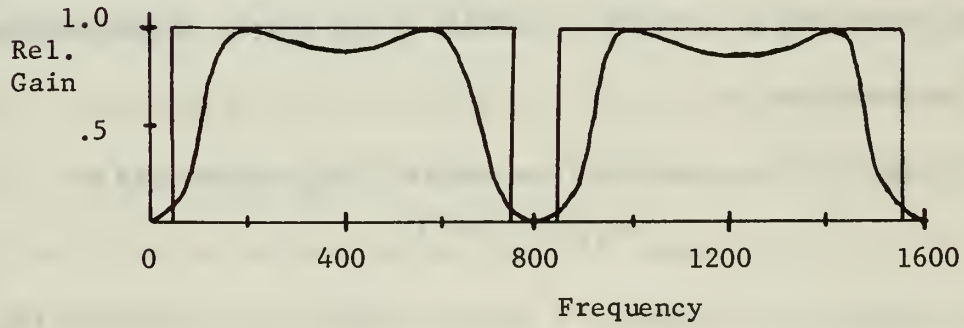

FIGURE 4: PARALLEL CANCELLATION

case as was done to generate the values used in Figure 4(b). The curve shown is a 2-pole characteristic. To produce a 3-pole characteristic using this method would require two more terms in the series and hence two more delay blocks in the diagram. This approach is easily instrumented using digital delay techniques as discussed in Ref. 5. The disadvantage of an analog circuit using this technique is that each incoming pulse must be stored for (in the case shown) four pulse-repetition periods and the output of each storage bin connected to the output adder with varying coefficients at varying times. This is an extremely difficult proposition requiring many more circuit elements than the method given below.

The second technique is equivalent to delay-line cancellation using sampled analog delay circuits rather than continuous delay lines and hence can utilize synthesis methods and mathematical expressions developed for delay lines. References 7, 8, and 9 present methods of synthesis of delay-line networks (comb filters) and illustrate the block diagram implementation of some transfer functions.

A necessary step in the synthesis procedure is development of an expression for the transfer function of a 3-pole Chebychev filter. Reference 7 gives the procedure for determination of the required transfer function in terms of the Z transform where:

$$Z = \exp(j\omega T)$$

so that $1/Z$ represents a time delay of T seconds. The width of the

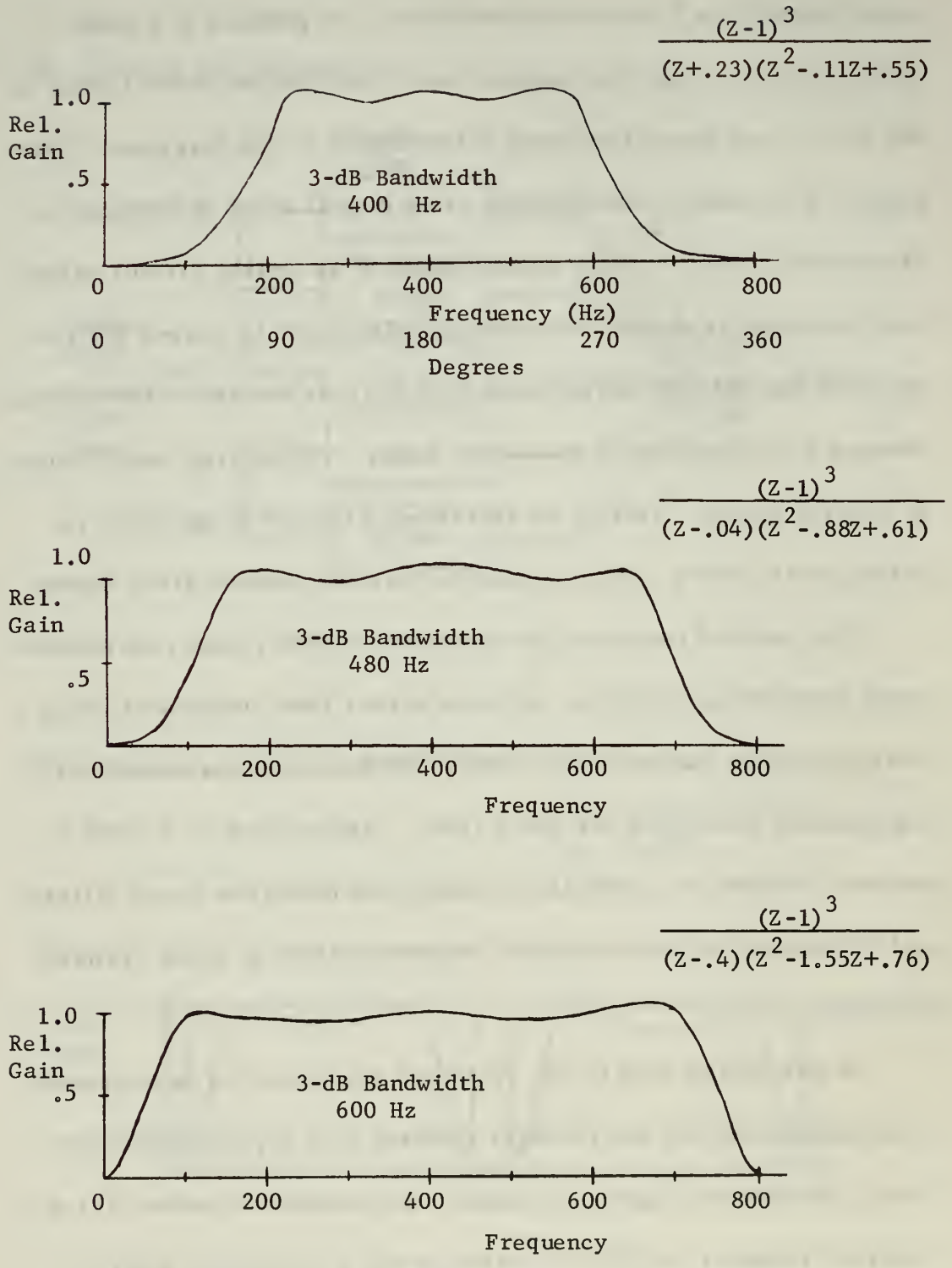

FIGURE 5: 3-POLE CHEBYCHEV FILTERS

passband of a cancellation filter can be varied while retaining the original filter characteristics by changing the coefficients of the denominator polynomial in the Z-transform representation of the filter. The three different transfer functions shown along with their respective frequency responses (which are repetitive at 800-cps intervals) in Figure 5 were derived from the same Chebychev low-pass filter characteristic. The frequency-response plots of Figure 5 correspond to Figure 4.24 (b), (c), and (d) of Ref. 1 with frequencies given for the AN/UPS-1 and in general terms for any pulse radar. The construction and testing of a filter with a characteristic like that of the middle one in Figure 5 is presented in Ref. 10.

Once the desired transfer function was known the next step was a block diagram synthesis of the desired filter. Perhaps the most familiar technique in the representation of transfer functions is the use of the Signal-Flow-Graph (SFG). This technique as applied to transfer functions of delay-line networks is illustrated in Ref. 8. In the case of any 3-pole transfer function derived from the same Chebychev characteristic (such as those in Figure 5) the transfer function is of the form:

$$\frac{(Z-1)^3}{(Z-A)(Z^2-BZ+C)}$$

This can be separated into two parts as a 1-pole filter in series with a 2-pole filter so that the synthesis can be done in two steps. The separation is shown below:

(a) 1-Pole

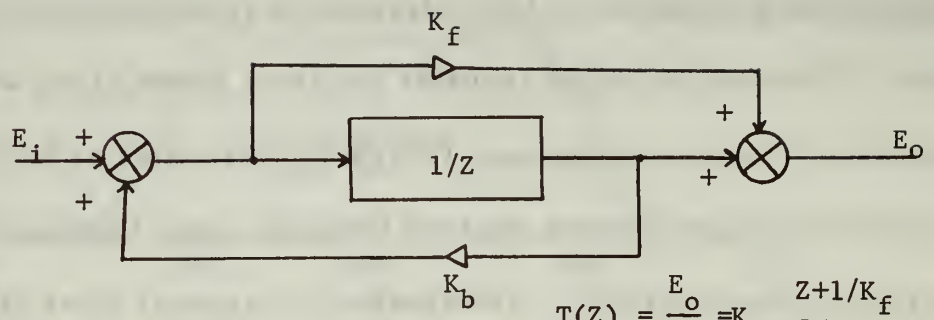

$$T(Z) = \frac{E_o}{E_i} = K_f \frac{Z+1/K_f}{Z-K_b}$$

(b) 2-Pole

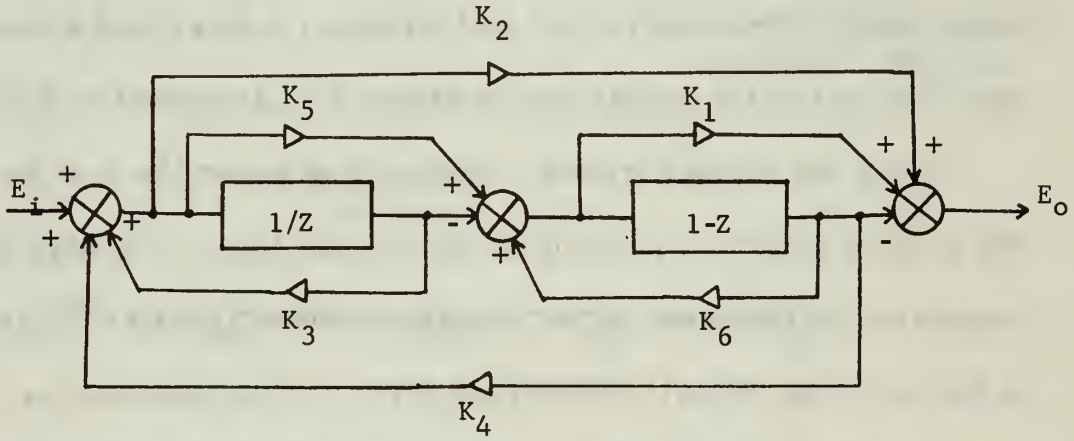

$$M_1 = \frac{-K_1-K_5-K_2K_6}{K_1K_5+K_2} \qquad M_3 = -(K_3+K_4K_5+K_6)$$

$$M_2 = \frac{1}{K_1K_5+K_2} \qquad M_4 = K_3K_6+K_4$$

$$T(Z) = (K_1K_5+K_2)\ \frac{Z^2+M_1Z+M_2}{Z^2+M_3Z+M_4}$$

FIGURE 6: GENERAL SFG REPRESENTATION OF TRANSFER FUNCTIONS

Values of Feedback Factors Required to Synthesize the Characteristics of Figure 5:

	A	C	(B-C)
(a)	.23	.55	-.44
(b)	.04	.61	.27
(c)	.40	.76	.79

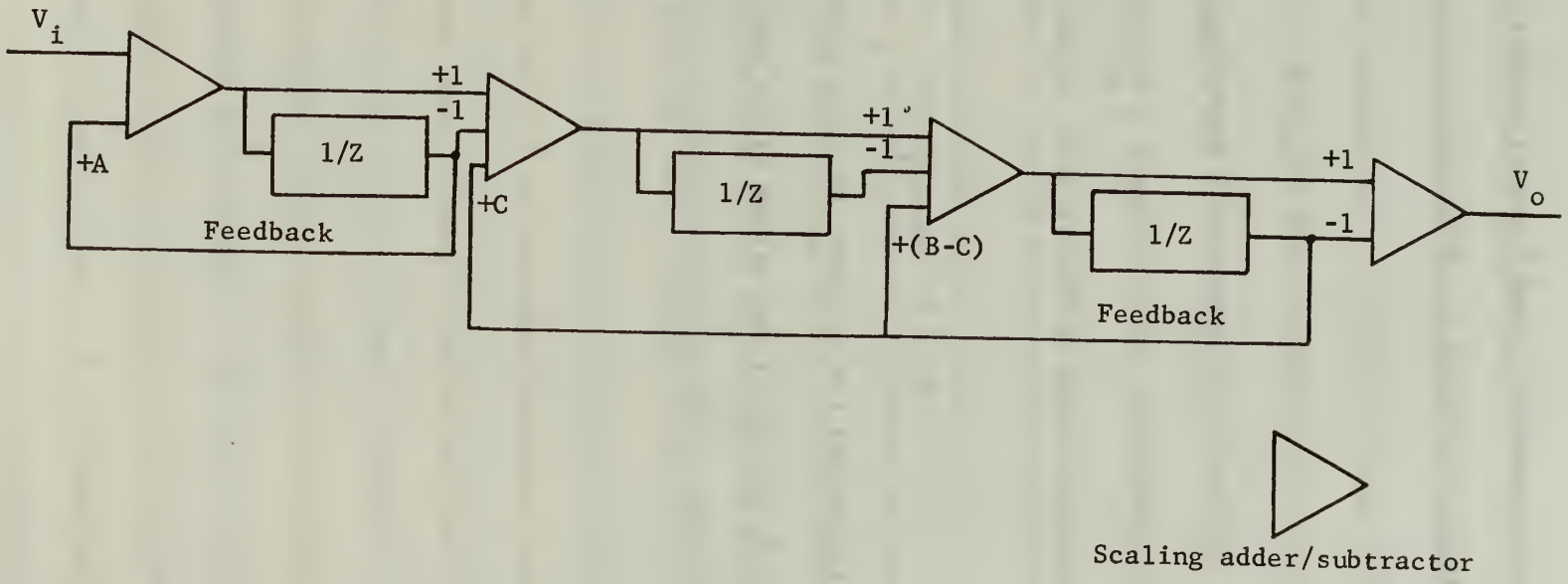

FIGURE 7: BLOCK DIAGRAM OF A 3-POLE FILTER

$$\frac{(Z-1)}{(Z-A)} \cdot \frac{(Z-1)^2}{(Z^2-BZ+C)}$$

The most general 1- and 2-pole transfer functions and their SFG's are shown in Figure 6. From this it is apparent that for the 1-pole case

$$K_f = -1 \quad \text{and} \quad K_b = A$$

produce the desired representation. The 2-pole block diagram (or SFG) representation can be formed in a number of ways dependent on the assumptions made in Figure 6(b). If the assumptions used are

$$K_2 = 0 \quad \text{and} \quad K_3 = 0$$

the block diagram for the transfer function given above is shown in Figure 7 which also gives the values of the feedback coefficients for representation of the transfer functions of Figure 5.

III. ANALOG DELAY

Once the block diagram of the desired filter was synthesized it was necessary to determine the methods to be used to actually construct each of the components. The delay shown as 1/Z in Figure 7 is the basic component of the system and methods to accomplish this delay had to be determined.

A. SIMULATED DELAY

It was found that by using a predetermined timing sequence a single analog sample-and-hold (S&H) circuit could act as an analog delay and that a certain class of transfer functions could be synthesized using this technique, which can be referred to as simulated delay. The restriction in the use of this method is that feedback cannot be utilized, which greatly limits its usefulness.

As an example of simulated delay consider the analog implementation of a single delay-line canceller frequency response. The input is the range-gated bipolar video of the radar and consists of a series of pulse returns from a target, separated in time by one pulse-repetition period. The amplitude of the pulses varies at the Doppler frequency of the target. The delay required to effect perfect cancellation must be exactly 1/PRF so that successive pulses are subtracted. If each short (1.4 microseconds for the AN/UPS-1) pulse is stretched out prior to introduction into the

(a) Stretched Input (Doppler Frequency 200 Hz for UPS-1)

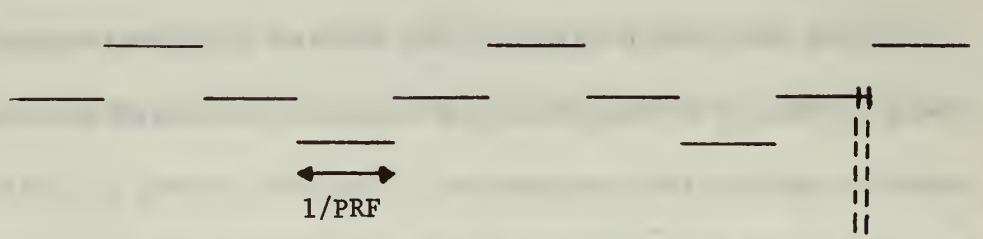

(b) Delay of (a) by a Sample-and-Hold Circuit

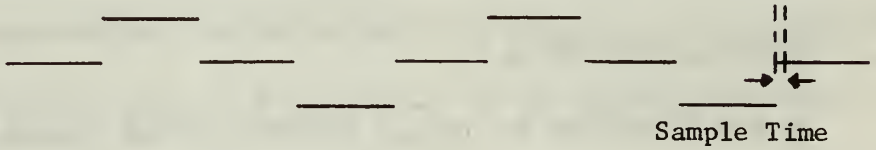

(c) Dual Delay-Line Canceller (Timing Shown)

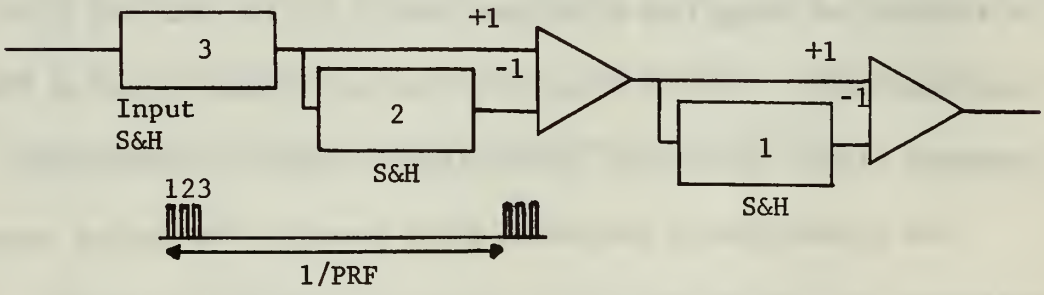

(d) Frequency Response of (c) and of a Single Delay-Line Canceller

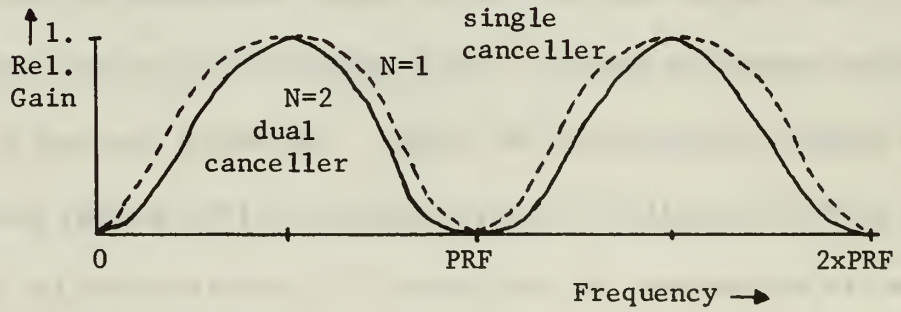

FIGURE 8: SIMULATED DELAY

canceller, so that the amplitude is held constant for the pulse-repetition period, the input to the canceller looks like Figure 8(a). If each of these pulses is sampled at the end of its duration and this value held for another pulse-repetition period the resulting waveform is shown in Figure 8(b). It can be readily seen that the waveform of this figure is the same as that of Figure 8(a) delayed by 1/PRF except during the sampling time, which can be made very short compared to the pulse repetition period. Thus if the delayed output of such a filter is subtracted from the input, the frequency response is the same as that of Figure 1(b) and if two such filters are cascaded as shown in Figure 8(c) with the proper timing the frequency response is the same as that of a dual delay-line canceller which is shown in Figure 8(d). The general expression for the Z-transform transfer function of N cascaded stages is shown below:

$$\frac{(Z-1)^n}{Z^n}$$

This produces a frequency response which can be expressed as:

$$\text{Gain} = \left|\sin^n\theta\right| \qquad \text{where: } \theta = \frac{PRF \cdot \pi}{F} \quad \text{(in radians)}$$

The cases N=1 and N=2 are illustrated in Figure 8(d). A filter using this technique was constructed and its frequency response recorded. The results matched the theoretical response.

When feedback was introduced into the filter the output became unstable due to a positive feedback loop which existed during the

(a) Block Diagram and Timing

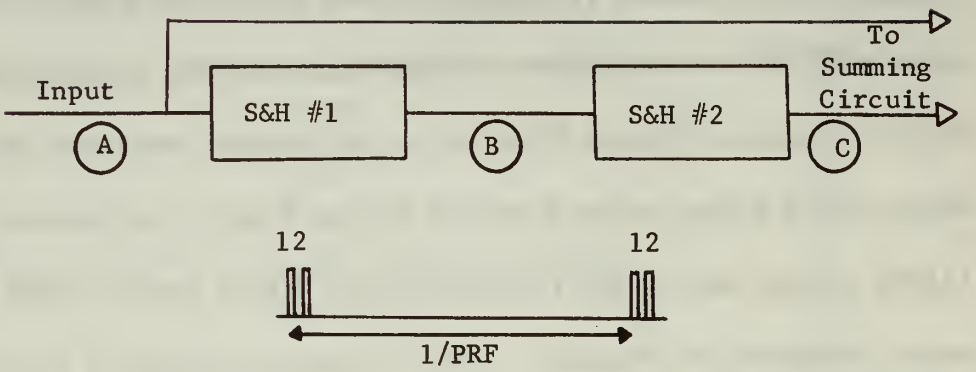

(b) Typical Waveforms

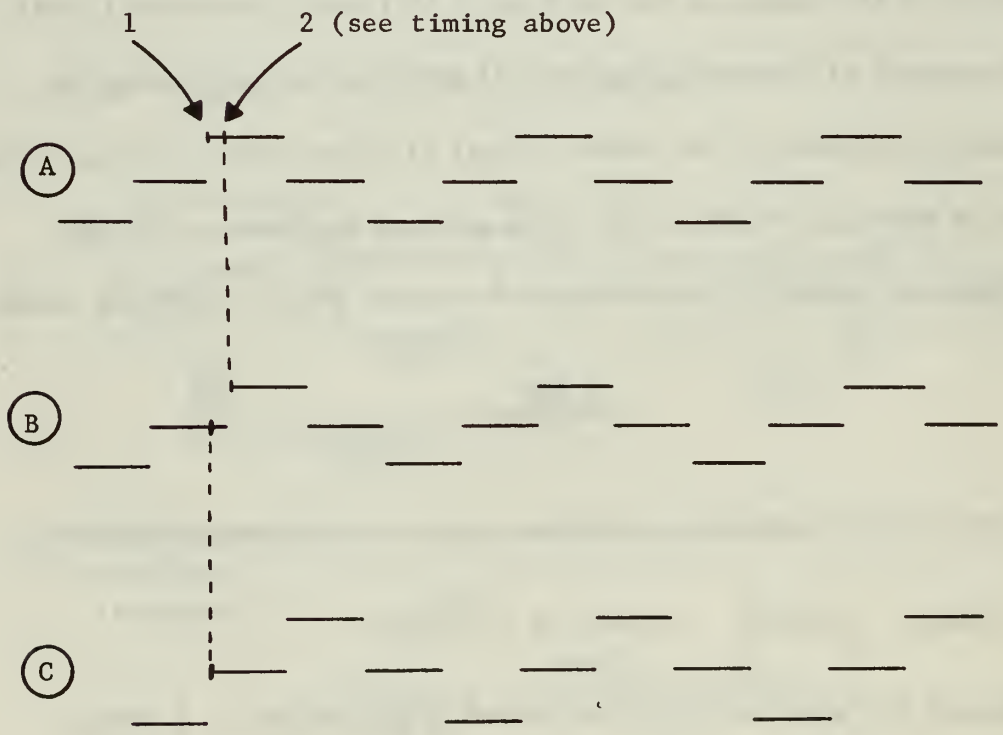

FIGURE 9: TRUE ANALOG DELAY

sampling time. Thus this approach proved to be of little value in the synthesis of Figure 7.

B. TRUE DELAY

To produce a true delay in a sampled system each sample must be held for a time equal to the pulse-repetition period in a way that provides buffering of the delayed pulse from the input pulses so that cancellation can take place and feedback can be used. To meet these criteria the delay was designed in two steps using two S&H circuits as illustrated in Figure 9. The input to the delay circuit is a waveform similar to that of Figure 8(a). This is sampled by the first S&H and held until the next input pulse at which time this value is transferred to the second S&H. The output of the second S&H circuit is thus always the input of the first delayed by one pulse-repetition period. The sample timing is also shown in Figure 9(a) and requires only two positive pulses. The first pulse is the same trigger which activates the range gate and the second pulse is delayed for any time less than one pulse-repetition period with respect to the first. Typical waveforms at the input, the output of the first S&H and at the output of the second S&H are shown in Figure 9(b). An important point to keep in mind is that the input to a S&H circuit is only open during the sampling time so that the value of voltage held by the first S&H is isolated from the input when the second one is sampling and is isolated from the output when the first one is sampling.

IV. FILTER CONSTRUCTION

To build a circuit having the desired characteristics required decisions on how to best implement the block diagram of Figure 7. A similar filter discussed in Ref. 10 used diode switching and discrete solid-state active components with ac coupling in its construction. The filter being designed had to be more flexible and have a better frequency response than that of Ref. 10 and hence new devices and techniques were sought to provide improved performance.

A. INITIAL CONSIDERATIONS

There are only two basic building blocks shown in Figure 7, an adder/subtractor and a delay. The components used in construction of these devices had to be linear, have a good frequency response (dc to several megacycles was desired in order to pass the fast rise time of the pulses and to produce good low-frequency response) and be readily available.

A very efficient device which met the requirement for use both as an adder and a subtractor is the integrated circuit operational amplifier (ICOPAMP or OPAMP). Another advantage of this device is that the input and output are isolated from the bias power supplies and thus dc coupling can be used which improves the overall low-frequency response of the circuit. A discussion of OPAMPS including types available, characteristics, and circuits used is contained in Appendix A.

The range gating and sampling necessary in the filter required a switch with fast turn-on and turn-off times and with a very high off-resistance and low on-resistance. The diode bridge meets these requirements as do switching transistors, but both must be biased and hence ac coupled. The Field Effect Transistor (FET) used as a switch requires no bias at the input and output (can be dc coupled), has zero offset voltage between input and output, is easily switched and was chosen for use in switching applications. Appendix B presents a discussion of FET switches including available types, switching characteristics and switching circuits used.

There were a large number of sample and hold (S&H) circuits which met the criteria required for construction of the delay element discussed in the last chapter. Four S&H circuits using FET switches and OPAMPS are discussed in Ref. 11. These circuits fit in well with the other circuitry selected and thus were chosen for use in the filter. Appendix C presents a discussion of the S&H circuits used and their performance.

B. CHARACTERISTICS

A circuit schematic of the final 3-pole Chebychev filter (corresponding to the block diagram of Figure 7 and the frequency responses given in Figure 5) constructed is shown in Figure 10. This illustrates the basic circuits and timing used and includes all active components but does not show biasing or frequency compensation which are shown in the Appendices.

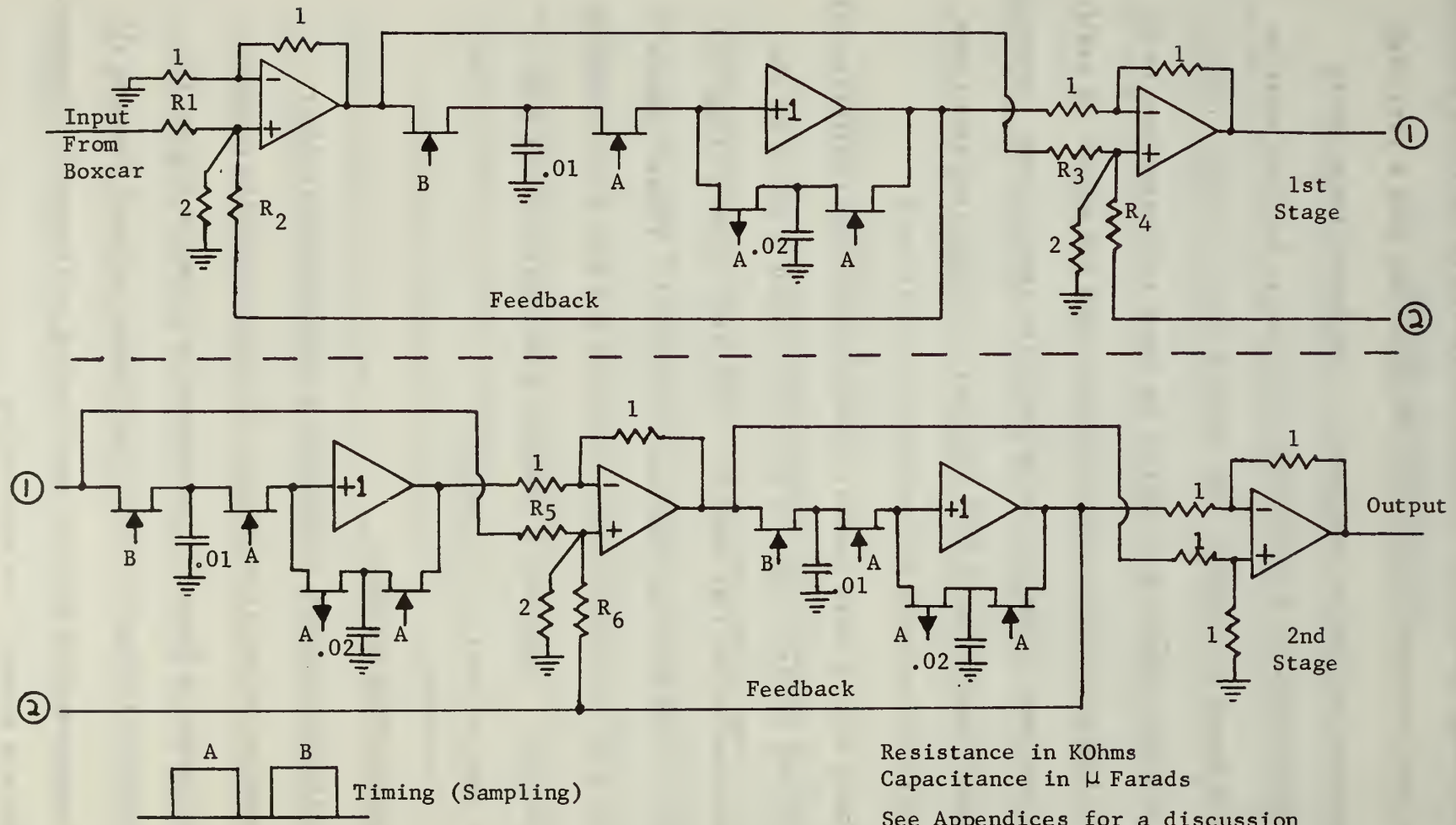

FIGURE 10: CIRCUIT DIAGRAM

Some of the important characteristics of the filter are shown below.

1. Gain: 2.9 (9.2dB)
2. Maximum input amplitude (peak-to-peak): 0.5 volts
3. Maximum output amplitude (peak-to-peak): 1.45 volts
4. The maximum amplitude of the repetitive frequency response of the filter is down 3dB at approximately 28kc due to the width of the sampling gate.
5. Power supplies required: 3

The experimental and theoretical frequency responses of the first and second stages are shown in Figures 11(a) and (b) and for the entire filter in Figure 12. The very close tracking of the experimental and theoretical responses indicates good cancellation and linearity in the filter as was required in the original design. The filter provides better than 40-dB attenuation at zero frequency and multiples of the PRF and can be easily modified to produce the other two filter characteristics of Figure 5. Modifications to vary the passband in several ways are discussed in the next section.

C. PASSBAND VARIATION

The discussion of filter characteristics in Chapter 3 indicated that a highly desirable feature of any MTI filter would be a variable passband. Two possible methods of variation are considered in this section and their performance, including ease of variations and frequency response, are compared.

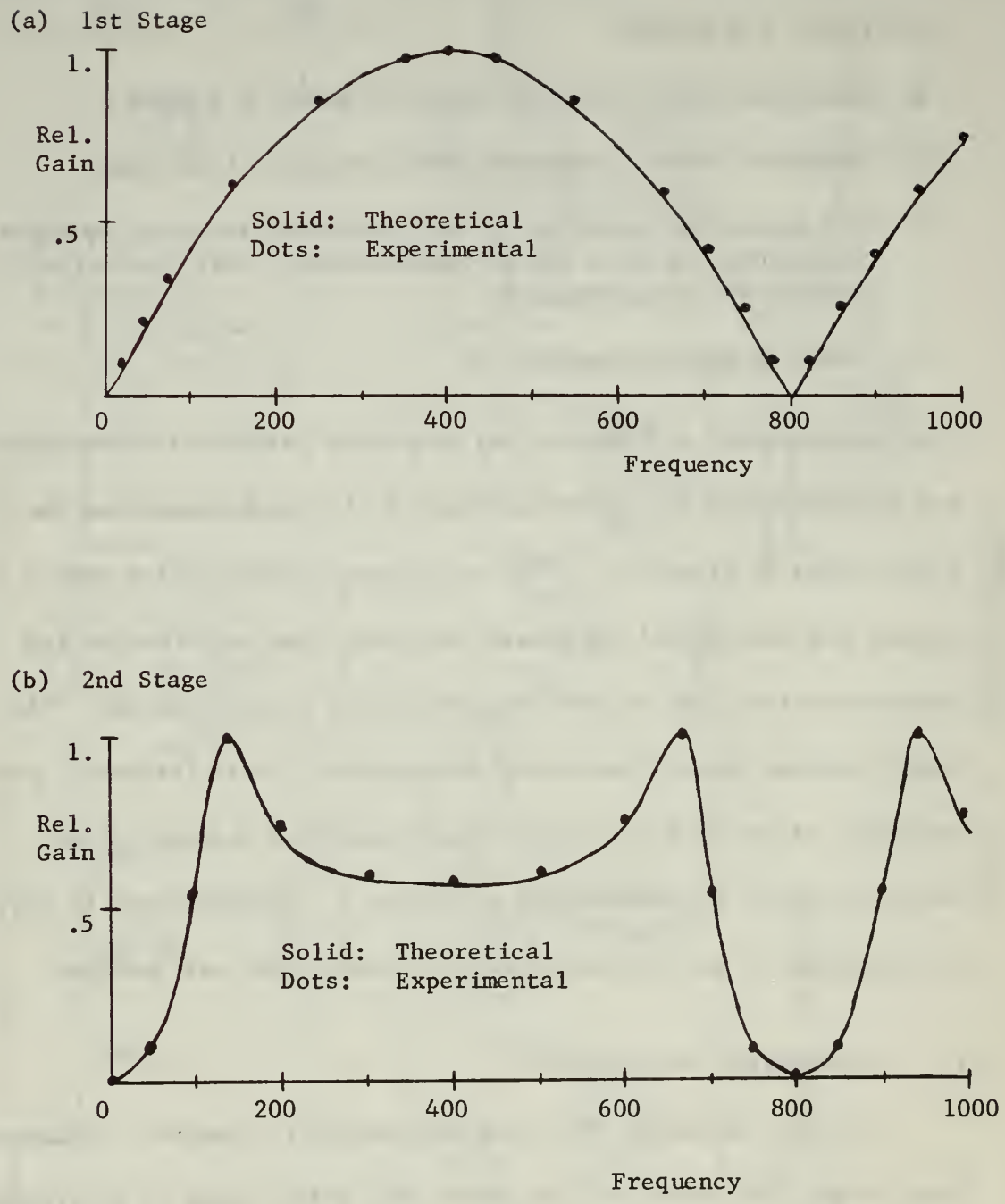

FIGURE 11: 1ST AND 2ND STAGE RESPONSE

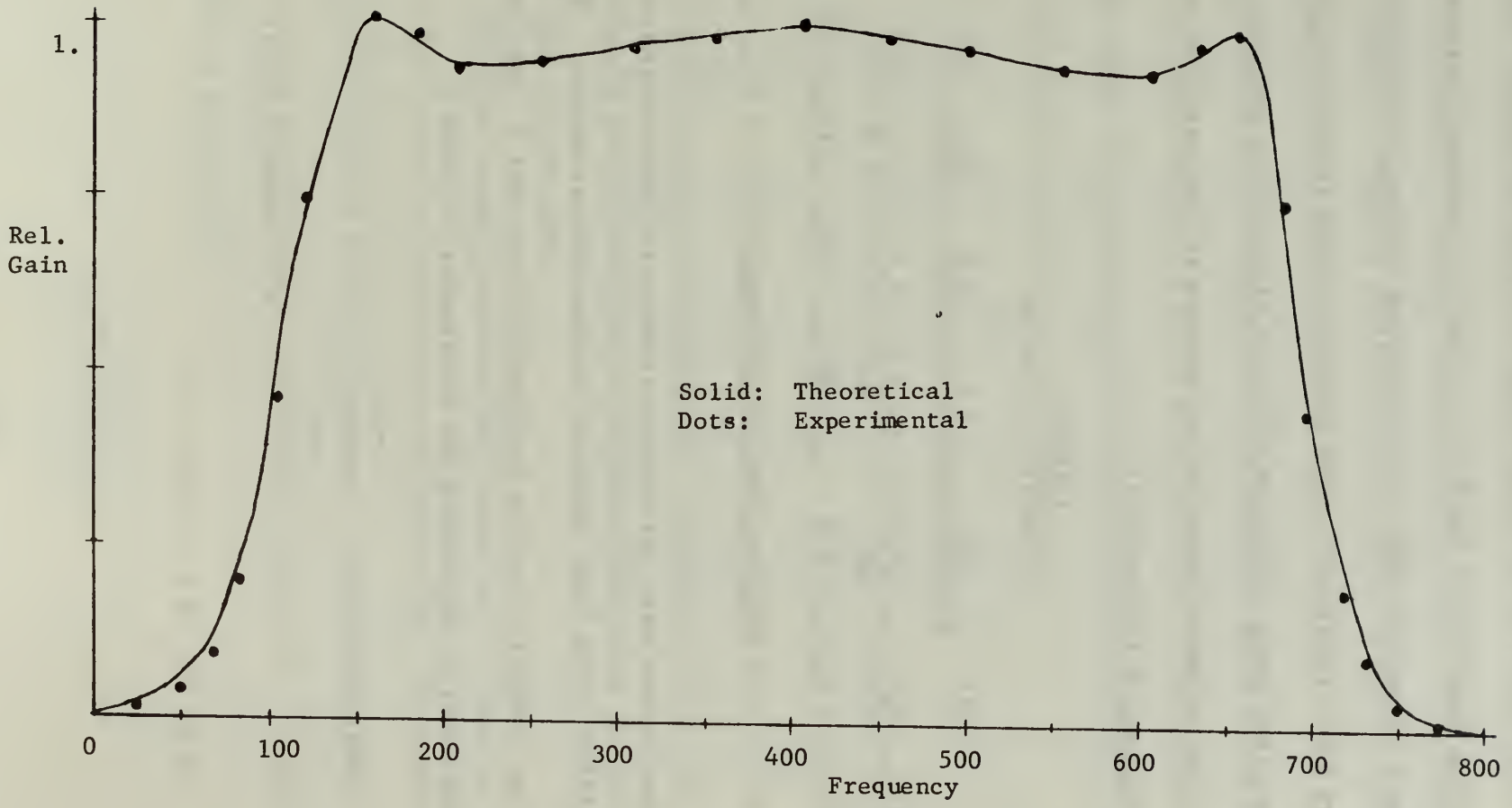

FIGURE 12: FREQUENCY RESPONSE OF THE ENTIRE FILTER

1. Chebychev Filter Method

The first method is variation of the feedback factors to change the bandwidth of the filter so that the frequency response remains a Chebychev type. This involves varying six resistors (R1 thru R6 in Figure 10). The resistor values required to produce the three frequency responses shown in Figure 5 are listed in Table I (the response given in the previous section used the second set of resistor values shown).

TABLE I
RESISTOR VALUES

	R1	R2	R3	R4	R5	R6
1.	1.5	6.7	.9	1.6	**	**
2.	2.0	48.	.68	1.2	1.6	5.1
3.	.8	3.0	.48	.68	.42	.53

Resistor values in kilohms

The above values were calculated assuming the input impedance of the OPAMPS in the unity feedback configuration as infinite. The gain of the OPAMP using the noninverting input was 2. The following equations apply in calculating the resistances in Table I.

$$R2,\ R4,\ R6 = \frac{1 - Y}{.5xY}$$

Y = Feedback factor

$$R1,\ R3,\ R5 = 2x(1 - Y)$$

To synthesize the upper frequency response shown in Figure 5 using the same circuit requires a change in the sign of the feedback factor which necessitates changing several internal leads and cannot be done simply by changing resistor values (which is why no values are shown for R5 and R6 in the first row of Table I). This method of variation of bandwidth maintains an optimum filter shape but is difficult to implement and hence would probably not be practical in a range-gated radar where several hundred filter bandwidths must be varied simultaneously.

2. Variation of Feedback Resistor Method

Any practical method of variation of the passband of the filter must be very easy to implement. This method involves only the variation of two resistor values (R4 and R6 in Figure 10) for each desired change in bandwidth and, although the filter is no longer of the Chebychev type, with proper design the passband shape can be quite good.

A further simplification of the circuit can be made by calculation of the transfer function of the Chebychev filter for which no feedback is required in the first stage. This eliminated the need for the first OPAMP adder/subtractor of Figure 10. The calculated function is given below.

$$\frac{(Z-1)^3}{Z(Z^2-.80Z+.60)}$$

TABLE II

VARIATION OF PASSBAND: EXPERIMENTAL RESULTS

Frequency (Hz)	1	2	3	4	5	6
5	.011	.015	.009	.011	.010	.020
10	----	----	----	----	.012	.050
20	.011	.015	.010	.016	.030	.130
30	----	----	----	.030	.070	.270
40	.012	.020	.016	.060	.125	.550
50	----	----	----	.110	.250	.750
60	.020	.050	.060	.195	.480	.999
70	----	----	----	----	.750	.999
80	.037	.100	.170	.600	.900	.850
90	----	----	----	.920	.870	.800
100	.070	.240	.400	.999	.850	.750
110	----	----	----	.999	----	----
120	.110	.400	.770	.920	.770	.730
140	.160	.550	.986	.850	.750	.740
150	----	----	.999	----	----	----
160	.220	.700	.986	.820	.760	.750
180	.290	.770	.960	.820	.780	.790
200	.360	.820	.940	.840	.810	.810
220	.450	.860	.930	.860	.850	.850
240	.550	.900	.940	.890	.890	.870
260	.620	.920	.950	.910	.900	.900
280	.700	.940	.960	.930	.920	.920
300	.790	.950	.970	.950	.950	.945
320	.850	.960	.980	.960	.960	.950
340	.910	.970	.990	.990	.970	.960
360	.950	.990	.990	.990	.995	.970
380	.980	.995	.995	.995	.999	.990
400	.999	.999	.999	.999	.999	.999
Gain:	10.	4.	2.9	1.9	1.7	1.3
R4		2.0	1.1	1.3	.8	.4
R6		6.0	5.1	.8	.79	.67

R1= N/A
R2= N/A
R3=.68
R5=1.6

Resistor values in KOhms

R1 thru R6 refer to Figure 10.

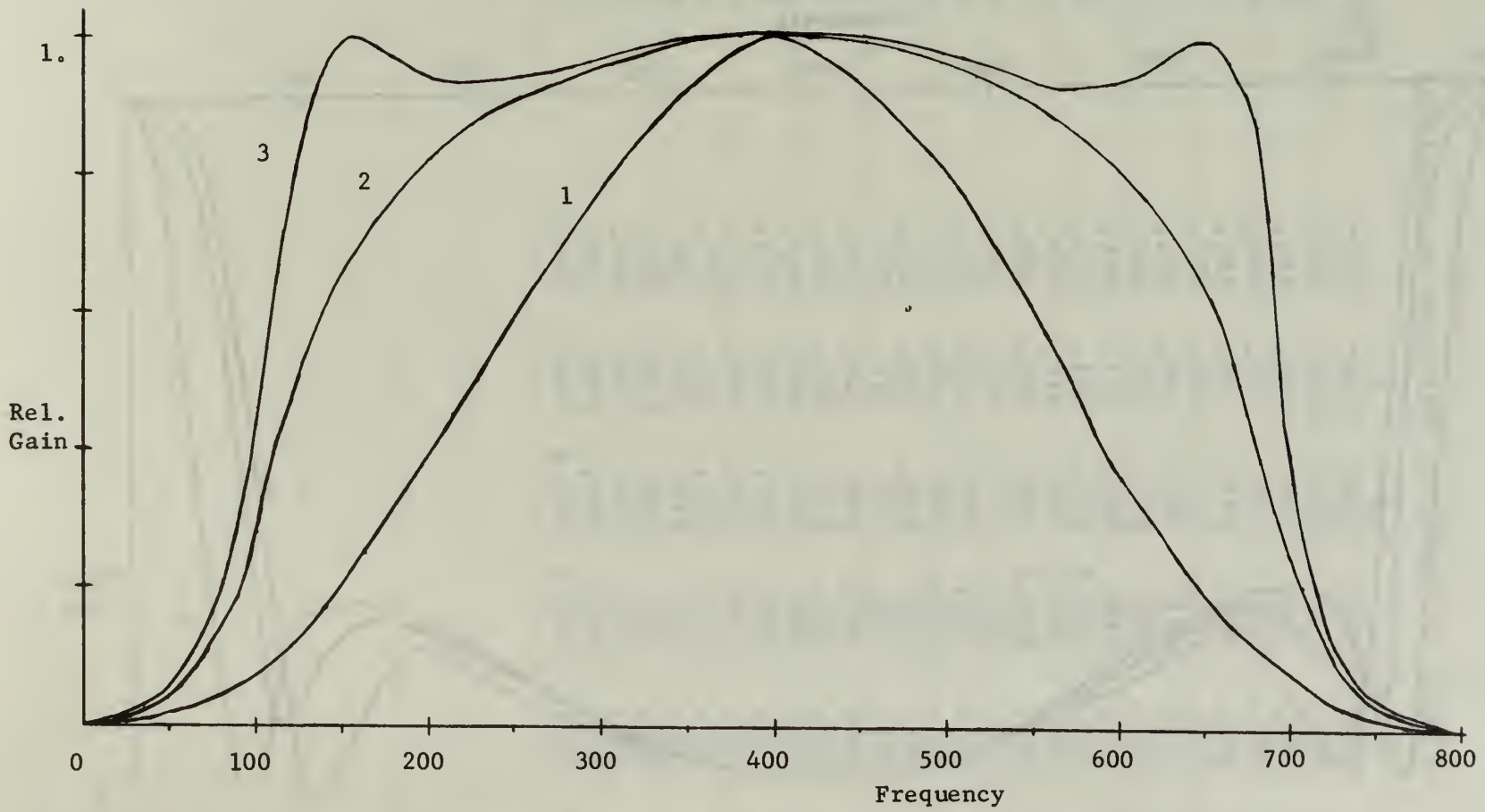

FIGURE 13: VARIATION OF PASSBAND I (EXPERIMENTAL)

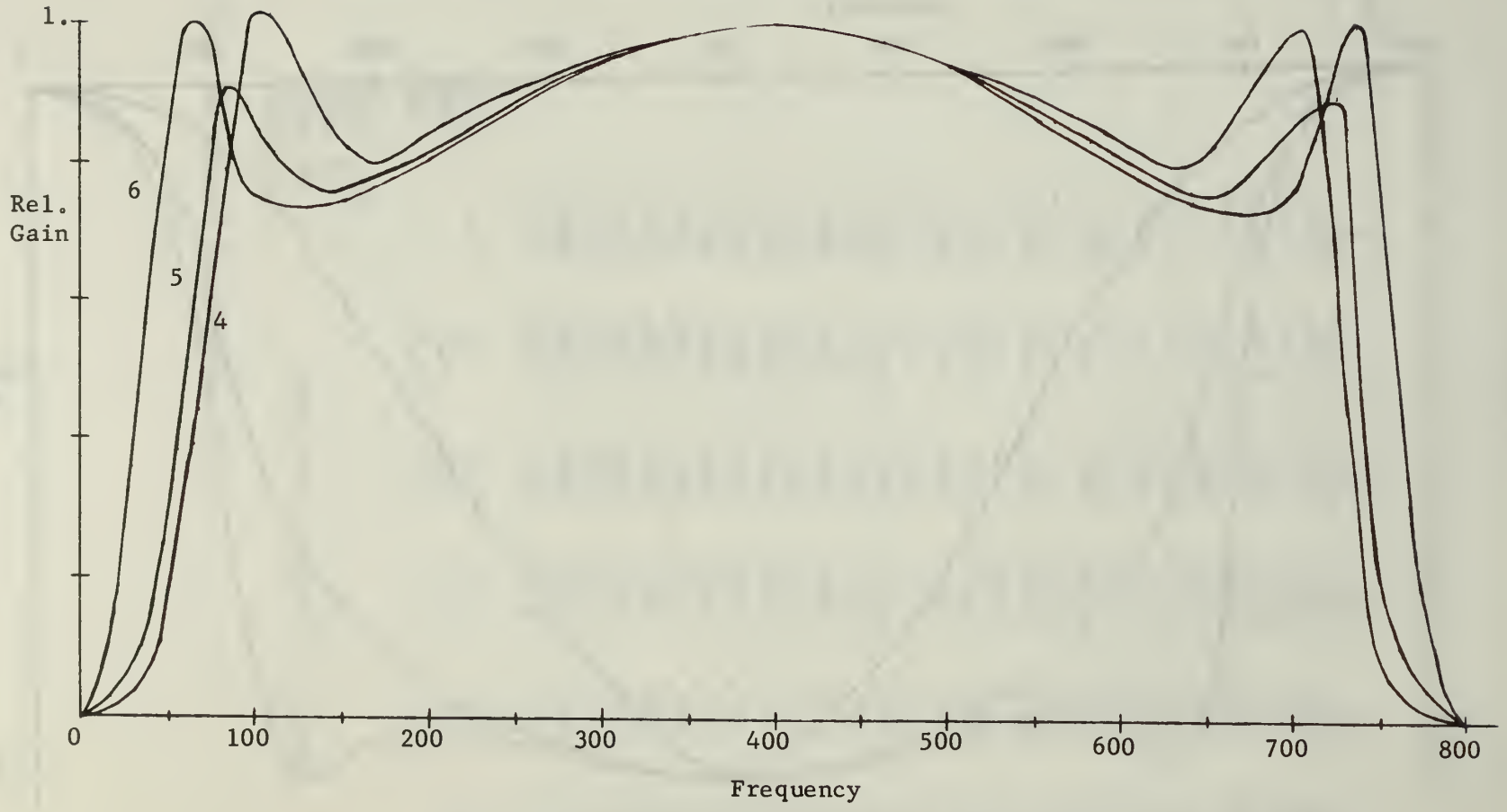

FIGURE 14: VARIATION OF PASSBAND II (EXPERIMENTAL)

TABLE III

VARIATION OF PASSBAND: THEORETICAL RESULTS

Frequency	1	2	3	4	5	6
0	.000	.000	.000	.000	.000	.000
10	.005	.0004	.0002	.003	.008	.033
20	.015	.002	.002	.011	.025	.092
30	.034	.006	.006	.026	.058	.209
40	.064	.013	.014	.053	.119	.459
50	.108	.024	.030	.101	.228	1.046
60	.169	.042	.055	.186	.431	1.668
70	.248	.069	.096	.338	.766	1.326
80	.350	.105	.158	.618	1.020	1.056
90	.475	.153	.252	1.100	1.000	.921
100	.626	.216	.389	1.160	.902	.850
110	.804	.292	.574	1.068	.834	.811
120	.101	.378	.776	.961	.795	.791
140	.150	.552	.984	.852	.766	.780
150	.179	.626	.987	.831	.764	.783
160	.211	.687	.969	.821	.769	.790
180	.282	.771	.934	.822	.788	.809
200	.361	.822	.919	.836	.814	.833
220	.446	.858	.918	.838	.842	.858
240	.534	.889	.925	.882	.871	.884
260	.624	.914	.936	.906	.898	.909
280	.711	.936	.951	.929	.924	.931
300	.791	.955	.964	.950	.946	.951
320	.862	.971	.976	.967	.965	.968
340	.920	.983	.986	.981	.980	.982
360	.964	.992	.992	.991	.991	.992
380	.991	.998	.998	.998	.998	.998
400	1.000	1.000	1.000	1.000	1.000	1.000

Implementation of this as the basic filter (the frequency response is the same shape as that of Figure 12 but has a bandwidth which is about 18 cps smaller) was accomplished prior to variation of the passband.

Because of the complications involved in calculating the best possible frequency response for variation of the resistors, the variation was done experimentally and six frequency responses corresponding to six different bandwidth filters were recorded. The results are given in Table II and plotted in Figures 13 and 14. These results illustrate a wide range of possible bandwidths with filters that are flat to within 3 dB across their passband and could be made readily adjustable by varying two potentiometers in each range channel to any of six preset values and by providing a circuit to compensate for the varying gain of the filter as the resistance values were varied. The transfer functions of each of the experimentally determined responses were calculated as shown in Appendix D. From the transfer functions, theoretical frequency responses were calculated and plotted using a computer and results are given in Table III. The results agreed closely with the experimental values.

D. SUGGESTED IMPROVEMENTS

The cancellation filter constructed performed in close accord with design requirements and theoretical expectations. A number of refinements or component improvements are possible, some of which would increase the effectiveness of the filter for use in a

range channel of a range-gated MTI radar and some which would decrease the number of components and hence the cost of the filter.

A simple gain-compensation circuit could be built (as mentioned in the previous section) which would provide a constant gain for a change in the shape of the frequency response of the filter. For the passband shapes determined in Section C the gain varies from 1.3 to 10.0 (as shown in Table II) so that gain compensation of a single amplifier should be sufficient.

An OPAMP with no dc input current requirement would eliminate the need for the approximately 3-microampere constant-current source at the positive input to the OPAMPS used in the high-input impedance S&H configuration. An FET input buffer before the OPAMP could provide a very high input impedance for the hold capacitor and also eliminate the constant-current source requirement, but ac coupling would be necessary.

The filter was designed for input signal levels from the AN/UPS-1 bipolar video and if handling of larger signal levels is required different components would be necessary. Design of the filter in integrated form (with the exception of the holding capacitors) would greatly reduce the size of each filter and improve the clutter attenuation by reducing the length of the leads.

V. TESTING THE FILTER ON THE AN/UPS-1 RADAR

In order to evaluate the completed filter more thoroughly it was necessary to compare it with a delay-line canceller in an MTI radar. The AN/UPS-1 has a delay-line canceller MTI capability with a range of about 80 nautical miles and was designed as a medium-range air-search radar. (The range in the non-MTI mode is somewhat greater.) The most valid comparisons were measurement of the minimum discernible signal and subclutter visibility with the same input signal to both the delay-line canceller and the range channel containing the filter. In order to make the comparison it was necessary to build the remaining components of a range channel in which the filter could be tested. The construction of these components is described in this chapter.

A. DESIGN AND CONSTRUCTION OF THE RANGE CHANNEL

A block diagram of the components required to build a complete range channel for use in a range-gated radar is shown in Figure 2(a). The primary considerations in design of the channel were that it be compatible with the filter in terms of signal levels and bias, and that the range channel be efficient enough to demonstrate the capabilities of the filter.

The input to the channel is the bipolar video output of the radar, and this must be sampled at a single range interval of 1.4 microseconds (which is the radar pulse width). If a target is

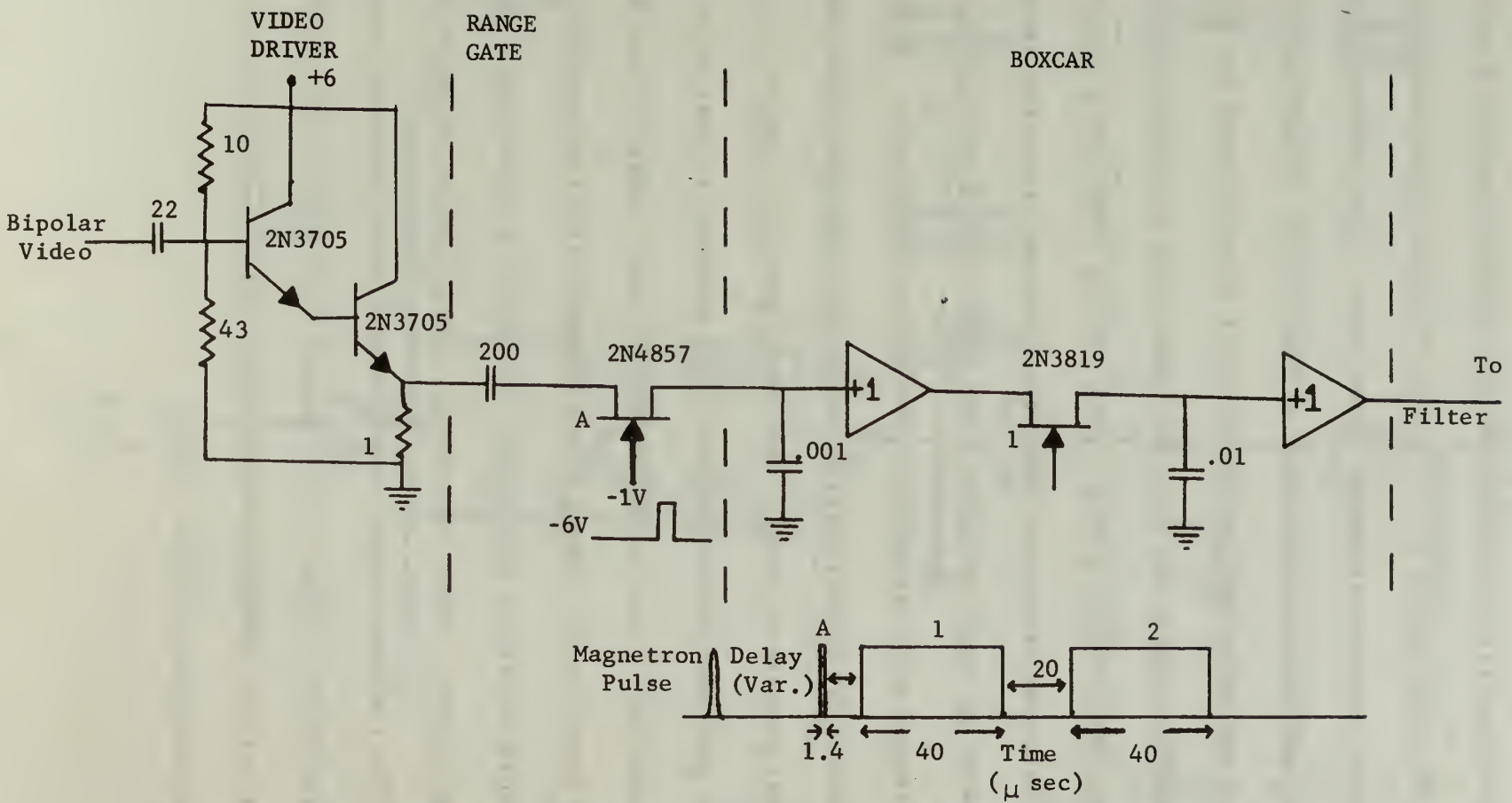

Note: Pulses 1 and 2 are same as in Figure 10

FIGURE 15: INPUT PORTION OF RANGE CHANNEL

contained within this range interval the value must be held for the pulse-repetition period of 1.25 milliseconds. This long hold to sample-time ratio requires the very rapid charging of a capacitor thru the range-gating switch and a very high-input-impedance buffer after the capacitor and prior to the filter. This holding circuit is the so-called boxcar generator of Figure 2(a). Reference 12 discusses the design and construction of a range channel and there a MOSFET input to the filter was used, thus accomplishing the holding efficiently in a single step. It was found that a boxcar built using the circuits of Appendix C did not have a flat enough hold with the short sampling pulse used and thus two sample-and-hold stages were cascaded to provide the input boxcar. Figure 15 illustrates the circuit diagram of the initial section of the range channel prior to the filter. The Darlington-pair input to the FET range gate provided the current drive required to charge the holding capacitor to the maximum value of input voltage during the short gating time. Only a single driver of this type would be required in an MTI by RGF radar, and hence it is not a part of the range channel. A variable-delay pulse generator triggered by the AN/UPS-1 system trigger was used to control the range interval covered by the channel. Real targets were tracked by adjustment of the variable delay (shown in Figure 15) to keep the range interval coincident with the target.

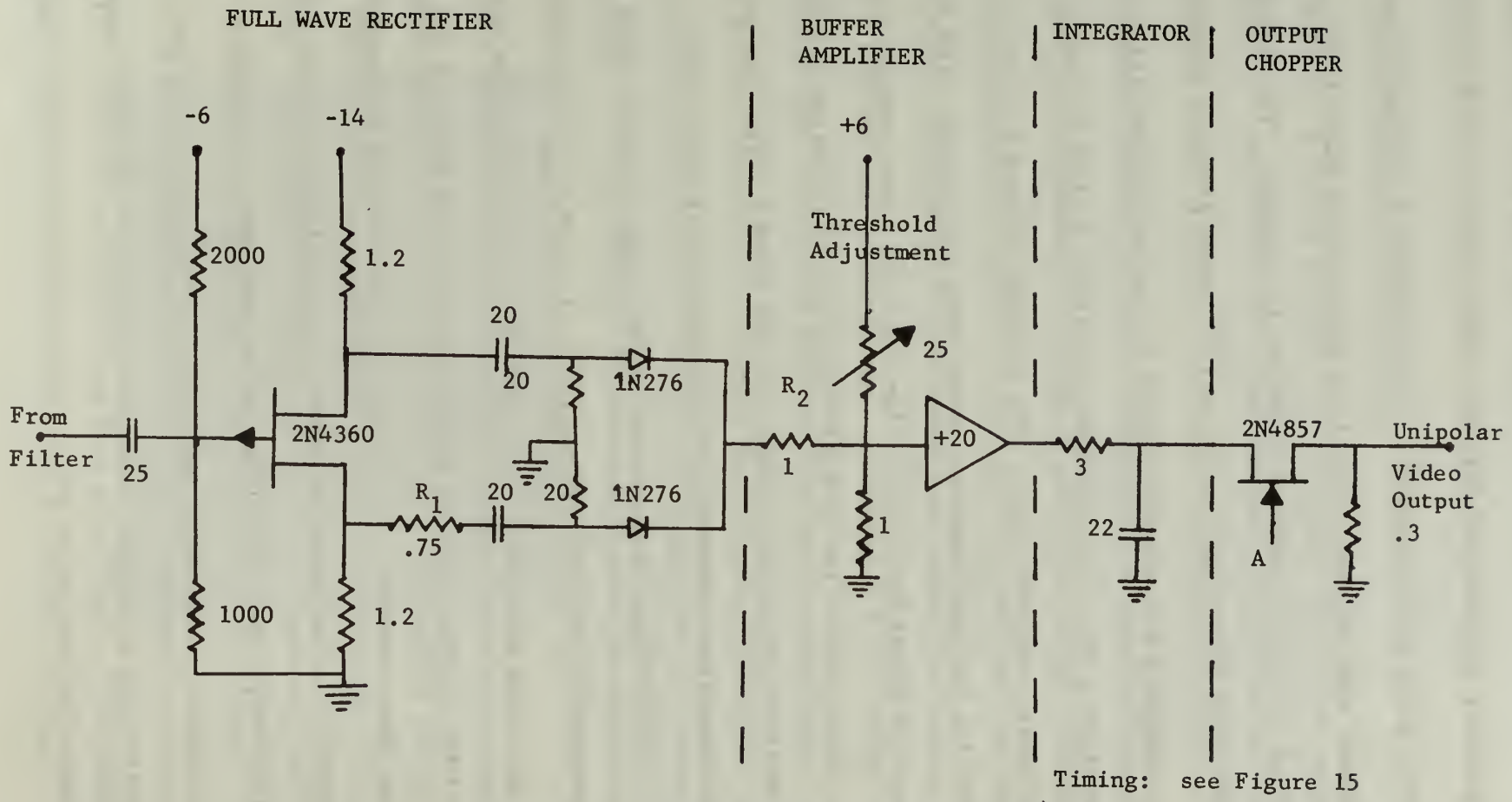

FIGURE 16: OUTPUT PORTION OF RANGE CHANNEL

The output portion of the range channel is shown in Figure 16 and includes a full-wave rectifier, an integrator, and a threshold detector prior to an output gate. This provides a unipolar output coincident with the input so that the output of the many range gates required in a radar could be combined for display. The full-wave rectifier was constructed using an FET which provided signals of equal amplitude but opposite sign at the source and the drain. These signals were fed into diode rectifiers so that the output was the full-wave rectified input. The resistor marked R1 is to equalize the driving impedance seen by the two diodes. The 1N276 Germanium diodes were chosen for their low offset voltage. The large voltage gain of the OPAMP was required to charge the long-time constant integrator to about 0.5 volt when a target was present. The optimum time constant of the integrator was determined (from considerations of maximum output signal-to-noise ratio for an exponentially weighted system (Ref. 1)) to be 65 milliseconds. Since the output impedance of the OPAMP is very small the discharge time constant with no signal present is the same as the charging time constant. The threshold detection was accomplished by adjustment of the variable resistor (marked R2 in Figure 16) so that the output was zero with a noise only input. The video reconstruction circuit was a switching FET turned on with the same pulse used to trigger the input range gate. This FET sampled the output of the integrator which was a positive dc voltage (0 for no

target) and hence the output was unipolar and suitable for direct combination with the other range channels in a system.

B. EXPERIMENTAL PROCEDURE

In order to validly compare the minimum discernible signal and subclutter visibility of the range channel with that of the delay-line canceller of the AN/UPS-1, it was necessary to be able to simultaneously observe the video output (both with and without MTI) of the radar video processor and the output of the range channel. For reproducibility of results a signal was injected into the radar from a signal generator. This allowed simulation of a moving target of any size and at any range. Tracking of a real target with the single range channel was possible (and was accomplished) but did not allow sufficient time to make the desired comparisons since aircraft moved rapidly out of the narrow range interval covered by the channel. A block diagram of the experimental set-up (which is similar to that used in Ref. 12) is shown in Figure 17.

The minimum-discernible-signal comparisons were made by displaying both the radar output (normal and MTI video) and the range channel output simultaneously on the dual-trace oscilloscope. The output of the simulated target generator was reduced until no target was visible on the oscilloscope from the radar output. The number of dB below this level at which the signal was still visible using the range channel output was then determined. The relative subclutter visibilities were determined in a similar manner.

FIGURE 17: EXPERIMENTAL SETUP

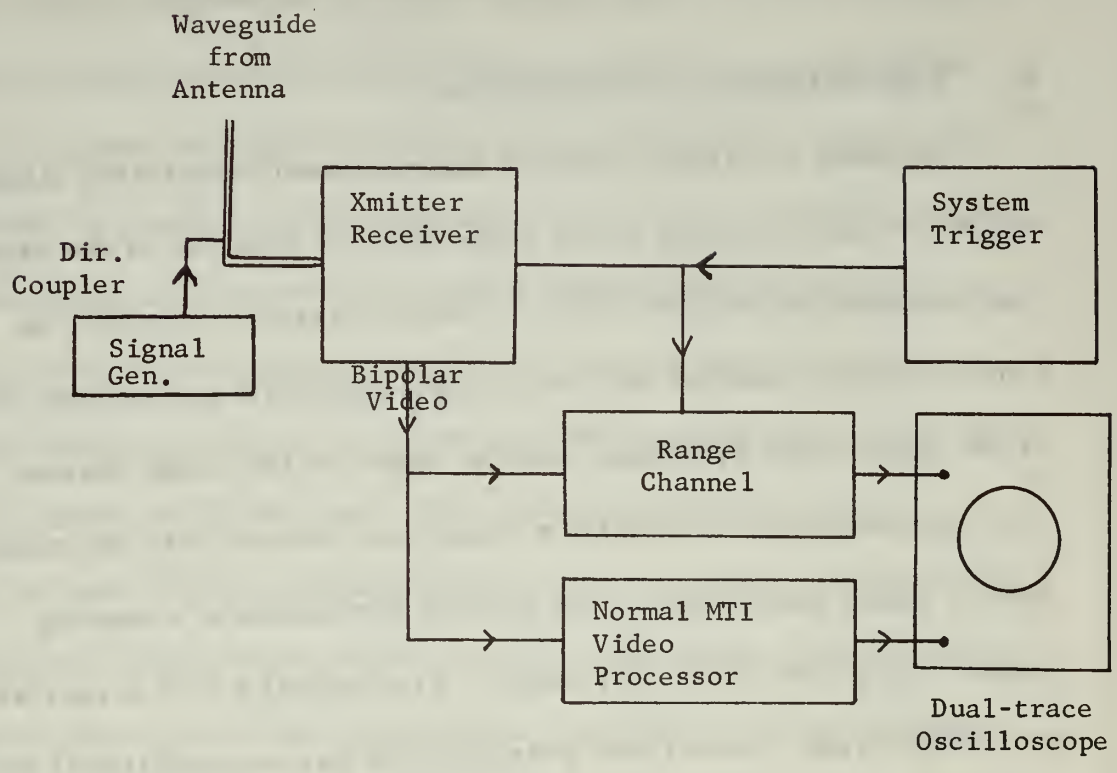

FIGURE 18: RANGE CHANNEL INPUT AND OUTPUT I

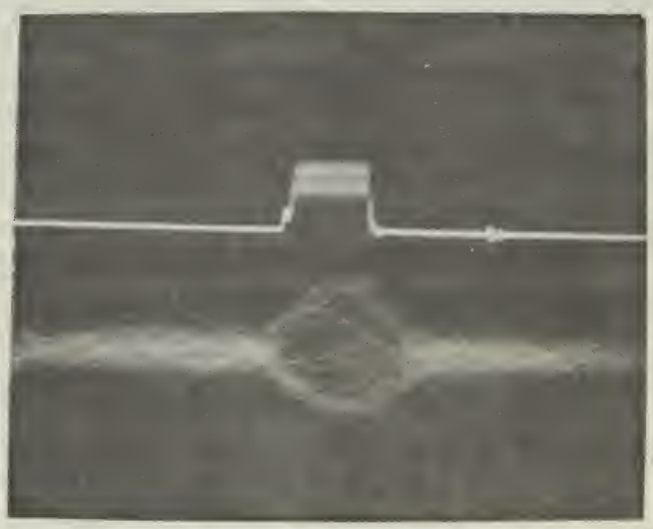

Relative measurements were used since absolute measurements are dependent upon a number of factors such as radar tuning, tuning of the signal source to the exact frequency of the radar, and experience of the operator. The comparative measurements taken should be reproducible as long as the systems are operated in parallel.

C. RESULTS

The experimental results determined upon comparison of the range channel performance and the performance of the AN/UPS-1 video processor are listed in Table IV.

TABLE IV

RADAR COMPARISON RESULTS

	Min. Disc. Signal	Subclutter Visibility
Normal video	10-dB improvement	N/A
Range channel	12-dB improvement	10-dB improvement

(MTI output is reference)

As mentioned previously the delay-line canceller MTI video processor degrades the signal-to-noise ratio of the input signal more than the normal video processor. In this test the minimum discernible signal of the MTI video was about 10 dB greater than that of the non-MTI (normal) video output which illustrated the extent of this degradation. With the range channel it was possible to discern a signal which was about 2 dB below that of the normal

video and 12 dB below that of the MTI video. This improvement is due to more efficient pulse cancellation in the filter than in the delay-line canceller.

An illustration of the output of the range channel gated ON for 1.4 microseconds with a 1.4-microsecond target return is shown in the upper portion of Figure 18. The blurred portion is due to noise and the indication that a target is present is the positive pulse (the center of the superimposed noise is the top of the pulse). The lower portion of Figure 18 is the bipolar video input to the channel which produced the upper picture as an output. A signal strength of -95 dBm was used in Figure 18 and the target is clearly visible in both pictures. Figure 19 shows the same two outputs for an input signal of -110 dBm. This time the target was not visible at the input to the range channel but is clearly visible at the output. This can be seen more clearly by comparing Figure 19 with Figure 20 which is the input and output for noise alone. Signals at levels lower than -110 dBm could be discerned in the range channel; however, noise fluctuations caused blurring and increased the difficulty of obtaining meaningful photographs. Figure 21 shows the MTI and normal video outputs of the radar for a -110 dBm input signal. The target was not visible in either case. This illustrates the superiority of the range channel in target detection since the same target was clearly visible when using it (Figure 19 (top)). The improvement in minimum discernible signal was due to several

FIGURE 19: RANGE CHANNEL INPUT AND OUTPUT II

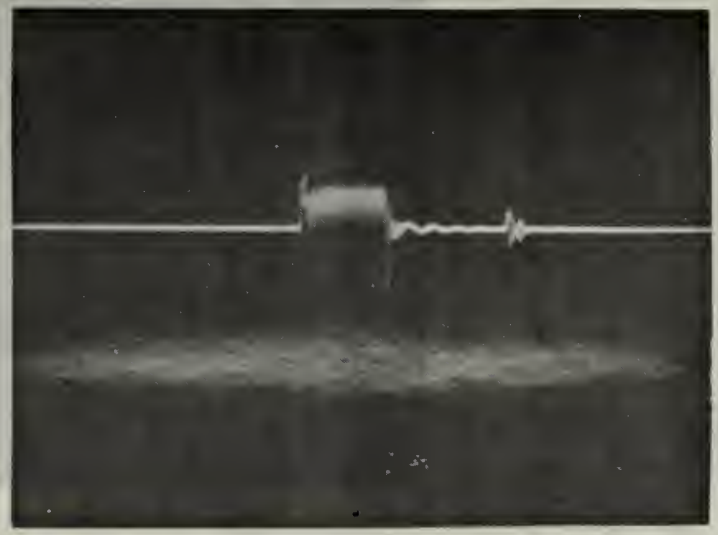

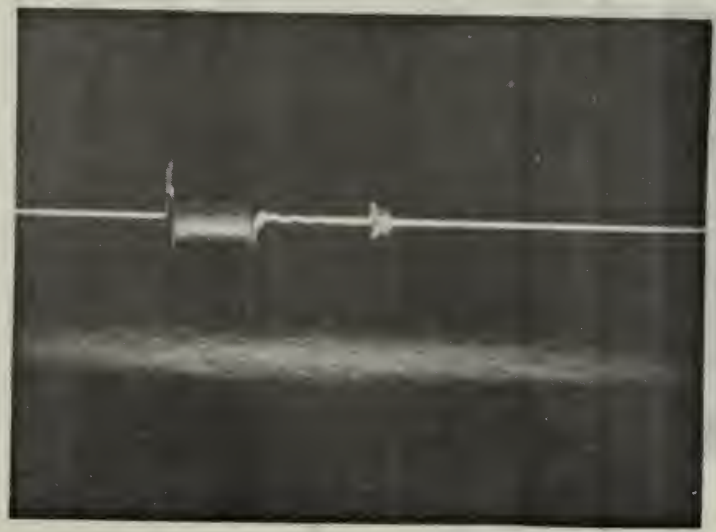

FIGURE 20: RANGE CHANNEL INPUT AND OUTPUT III

FIGURE 21: MTI AND NORMAL VIDEO OUTPUT

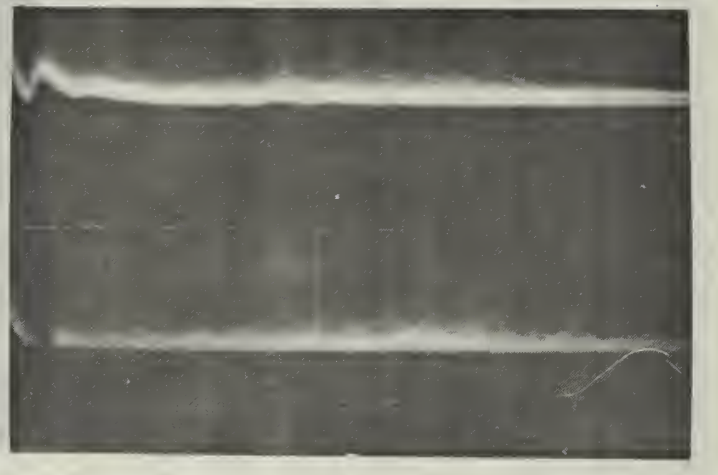

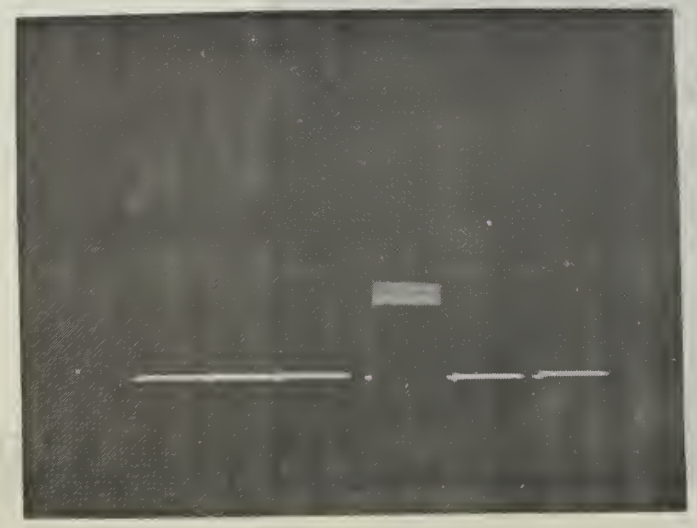

FIGURE 22: SIMULATED RANGE-GATED RADAR OUTPUT

factors including more efficient integration in the range channel and the lower noise figure of the solid-state circuitry compared with the delay line and its associated circuits.

Noise effects can be eliminated in the video presentation of a range-gated radar by adjustment of the threshold detector in the range channels. In addition, the integration of all of the pulses returned from a target during the time the target is within the radar antenna beamwidth smooths out noise effects. Thus an oscilloscope presentation of the output of a series of range channels would be free of noise, and if a target were present it would be readily identifiable. This is illustrated in Figure 22 which shows a simulation of the output of six consecutive range channels. One of the output intervals in the figure indicates that a target is present and there is some noise superimposed on the output pulse. The clear indication that a target is present with no noise appearing in adjacent range intervals is indicative of the quality of the output display of a range-gated radar.

As a target passed between two range intervals the amplitude of the output pulse would gradually decrease in the first interval and increase in the second until the target disappeared completely from the first interval. This is a gradual process so that it is possible for a single target to activate two range channels simultaneously. Hence a target should be visible at all times. At the maximum range of the radar, however, a target return may be

large enough to show up while in the center of a range interval and not be large enough to activate the threshold detector of either channel while between two intervals. A momentary loss of a target could occur in this case.

VI. DISCUSSION OF RESULTS AND CONCLUSION

The variable-bandwidth filter constructed produced a desirable Doppler frequency response which could be used to eliminate clutter in a variety of environmental conditions. An example of the usefulness of such a filter would be in detection of aircraft flying low over water, which might be hidden by sea clutter if a less effective filter were used. The greater than 40-dB attenuation of the filter at multiples of the PRF was better than many currently used MTI radars and could be improved by using printed-circuit or integration techniques which would reduce spurious responses introduced by long leads used on the vector board model which was constructed.

The number of active components required to construct this 3-pole filter is larger than the number required for a comparable 3-pole bandpass filter (Ref. 3).

A number of range-gated search radars have been built which provide considerably increased performance over comparable delay-line MTI radars (Refs. 2 and 4). None were found to have variable-bandwidth 3-pole filter characteristics or to use the type of filter discussed in this paper, probably due to the increased complexity and hence cost of the required circuitry.

The filter and range channel constructed allow variation of pulsewidth with no effect on filter characteristics.

The Doppler characteristic shown in Figure 1 (b) as the ideal response is for a single PRF and has frequencies at and around multiples of the PRF at which no target would be visible. The velocities corresponding to these frequencies are known as blind speeds and can cause loss of a target. A technique developed to eliminate blind speeds is use of a variable interpulse period (VIP) so that, for instance, groups of five consecutive pulses would have different interpulse periods. VIP cannot be readily used on delay-line canceller radars. This technique is applicable to the range channel and filter constructed and the results of such a variation are easily calculated since the filter shape remains the same and only the bandwidth changes for different PRFs. Hence addition of the frequency responses for each PRF and normalization of the result yields the VIP frequency response. Reference 5 discusses the VIP method used for elimination of blind speeds.

The conclusions reached upon completion of the construction and testing of the filter and associated range channel were that this concept provides a high-performance, solid-state, range-gated radar which is very flexible. With modern LSI techniques such channels could be used to greatly reduce the size of the video-processing unit of a delay-line canceller type of radar with a simultaneous increase in performance.

APPENDIX A

Operational Amplifiers

Integrated-circuit operational amplifiers (ICOPAMPS or OPAMPS) are linear amplifiers having very high open-loop voltage gain. In addition, OPAMPS have the following properties:

1. Bandwidth from dc to some upper 3-dB frequency (which is dependent on the quality of the OPAMP and the feedback used).
2. High input impedance.
3. Low output impedance.
4. Low noise figure.
5. Low offset (voltage and current).
6. Small drift.

OPAMPS are used to perform many different operations including integration, differentiation, summation, and subtraction. A complete discussion of OPAMPS including equations for calculation of various parameters, feedback circuits and frequency compensation is contained in Ref. 13.

The device characteristics required for the circuit designed were high input impedance, low output impedance, rise and fall times of less than 0.5 microseconds, variable gain (0 dB to 20 dB) and capability for use as a scaling adder/subtractor. The ICOPAMP adequately met all of these requirements.

The two available OPAMPS (the Fairchild μA-709 and the RCA CA-3029) were tested and compared. The data sheets (Refs. 14 and 15) and calculations using equations from Ref. 13 indicated the following pertinent characteristics:

	μA-709	CA-3029	units
Power supplies	± 18	±6	volts
Input (open loop)	100	14	Kohms
Input (unity gain)	100*	15*	Mohms
Output (open loop)	150	75	Ohms
Output (unity gain)	0.05*	0.2*	Ohms
Open loop gain	40000	1000	
Rise time	0.3	0.16	sec
Percent overshoot	10	small	
Bandwidth (unity gain)	0.7	10	MHz

*Calculated

Tests made on two units of each type showed the values given above to be accurate except that the rise time of the 709 was greater than 0.3 microsecond. Since the circuit must pass fast rise-time pulses the CA-3029 was chosen for use although its input and output resistances were not as good as the 709 and hence its performance in S&H circuits not as good.

The CA-3029 comes in a 14-lead dual-in-line configuration. The terminal connections used in the unity-gain configuration are shown in Figure 23 (a). For a gain greater than one, the only changes required are addition of a feedback resistor and different frequency compensation between terminals 9-10 and 1-14, as shown in Ref. 13. The resistor and capacitor used for frequency compensation from terminal 11 to ground were adjusted for optimum rise

time and are required for stability in the unity-feedback configuration only. The current source shown in the figure is necessary when used in a S&H circuit to provide a flat hold since a 3-microampere dc input current is required by the device. This can be provided by a large resistor and high-voltage source (as was done) or by use of an FET input stage.

Figure 23 (b) shows the terminal connections for a scaling adder/subtractor configuration and the symbol used in Figure 10 for this utilization of the device. The equation for the output voltage in terms of the input voltages, assuming zero source impedance for each input (which is a good assumption since the input voltages all come from other OPAMPS in the unity-gain configuration) is given below.

$$V_o = -\frac{1}{R_1}V_1 + 2 \cdot \frac{R_3 // R_4}{R_1 + R_3 // R_4} V_2 + 2 \cdot \frac{R_2 // R_4}{R_3 + R_2 // R_4} V_3$$

R in kilohms

// = in parallel

This equation was used in conjunction with the transfer function derived in Appendix D to derive the theoretical responses given in Table III.

The approximate input resistances seen by the sources V1, V2, and V3 of Figure 23 (b) are given below as R1, R2, and R3 respectively.

$$R1 = R_1 + 1$$

$$R2 = R_2 + R_4 / / R_3$$

$$R3 = R_3 + R_4 / / R_2$$

The CA-3029 provided excellent results in all circuit configurations in which it was used.

(a) Unity Gain Configuration

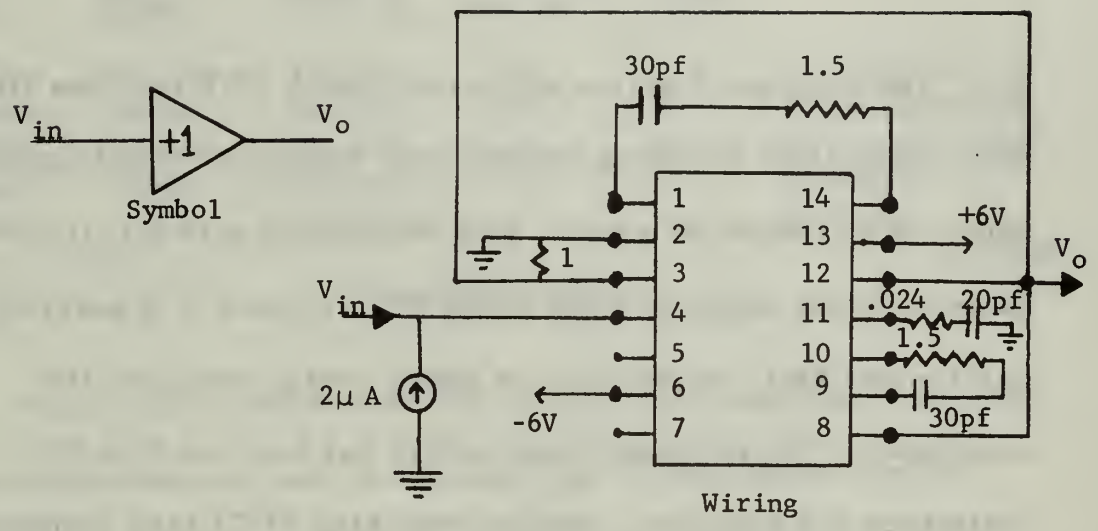

Resistance in KOhms

(b) Scaling Adder/Subtractor Configuration

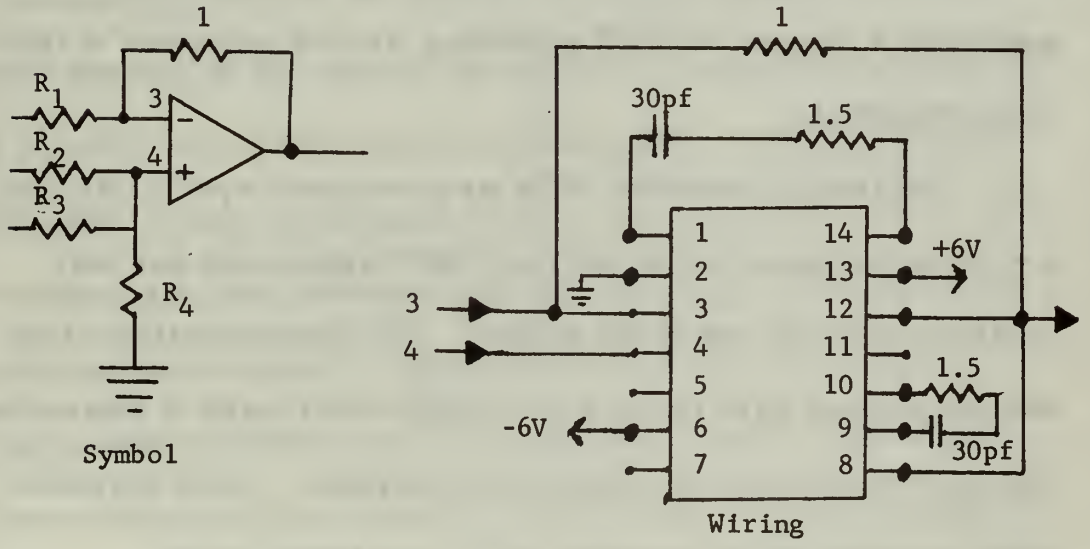

FIGURE 23: OPAMP TERMINAL CONNECTIONS

APPENDIX B

Switching with FETs

The principle features which distinguish FET switches from other solid-state switching devices are: simplicity of operation, ability to dc couple the switch, bias required at gate only (if enhancement and depletion mode MOSFETs are used it is possible to eliminate bias completely), no offset voltage and high OFF resistance. The principle disadvantage has been too high ON resistance and high cost. Modern switching FETs have improved characteristics so that they are highly competitive switching devices and are being used to a greater extent in modern instrumentation. There are basically two types of FETs in use, the Junction FET (JFET) and the insulated gate FET (MOSFET). Reference 16 provides a general discussion of FETs and Ref. 17 contains examples of a number of JFET switching circuits and some of their characteristics.

The readily available FETs were not made specifically for switching purposes except for the 2N4857 type which was only available near the end of the project. The characteristics of the devices at hand were checked and simple tests made to determine the one with the best switching characteristics. Some pertinent characteristics of the available FETs are shown below.

Type	R(ON) (Ohms)	R(OFF)* (MOhms)	Turn on Time (μ sec)	Max. signal (volts)	
2N3819	140-300	10-100	.2	1.5	N channel JFET
2N4857	25-40	10-100	.006	1.5	N channel JFET
2N4360	160-180	10-100	.5	2.0	P channel JFET
40468	1000	100-1000	---	---	MOSFET
3N141	1000	100-1000	---	---	dual-gate MOSFET

*Theoretical value

The 2N3819 and 2N4360 FETs were sorted and those with minimum ON resistance used in the switching circuits since low ON resistances were required. The 2N4857 was used in circuits requiring very low ON resistance and fast switching times when it became available. Figure 24 shows the switching circuits used for the three types of FETs employed as switches.

The value of input resistance of the stage following the FET switch shown in Figure 24 results in an output greater than 0.9 (or 90 percent) of the input to the switch. In analysis of the switching circuits, one simply uses the ON and OFF resistances of the FET used. These resistances do vary with amplitude of the signal, but with a high input resistance of the next stage the small change in ON resistance does not appreciably affect the output unless large signals (greater than 1.5 v) are used. Due to capacitance between the source and drain the rise time of the switching pulse should be greater than 0.1 microsecond for the 2N3819 and 2N4360 to prevent the presence of a small switching transient at the signal input.

(a) 2N3819 N-Channel JFET

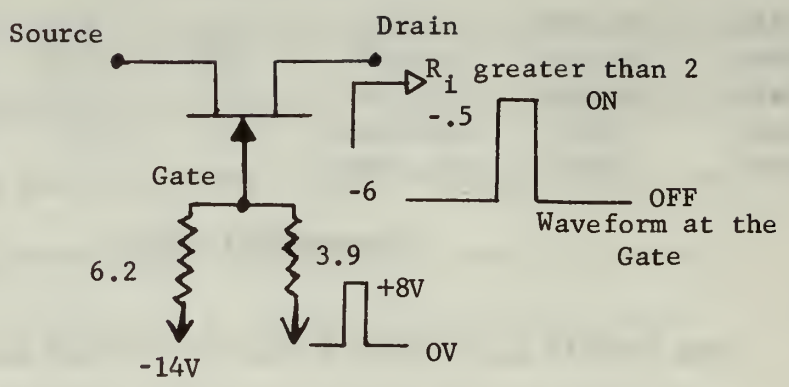

(b) 2N4857 N-Channel JFET

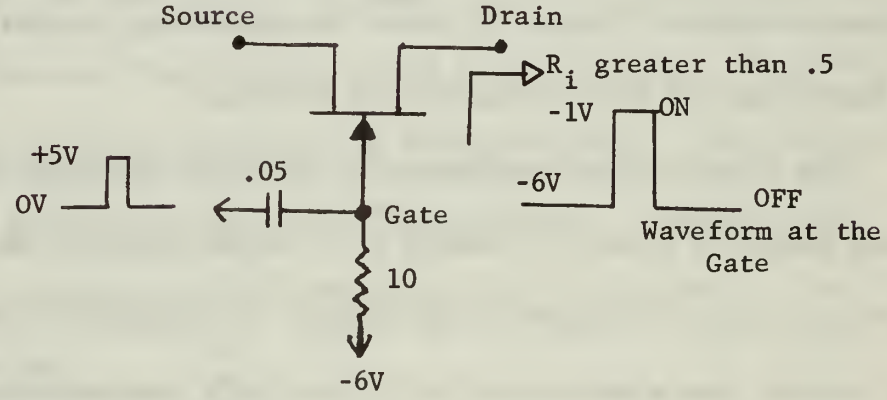

(c) 2N4360 P-Channel JFET

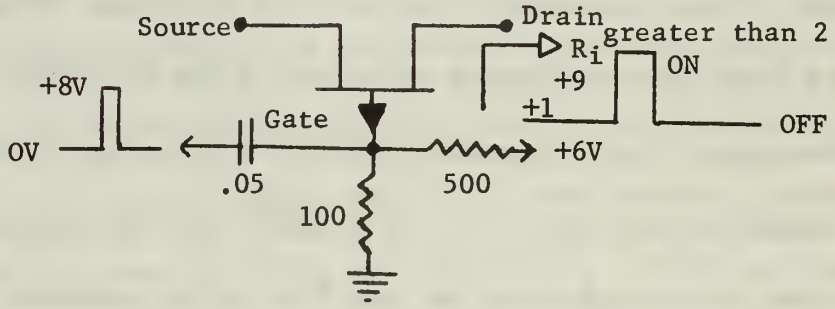

FIGURE 24: FET SWITCHING CIRCUITS

APPENDIX C

Sample-and-Hold Circuits

The sample-and-hold (S&H) circuit is basically a timed switch connected to a storage element so that any input can be sampled and the sample voltage held on the storage element until a new sample is taken. Capacitors were used as the storage elements and FETs as the switches in the implementation of the S&H circuits. A basic S&H using these components is shown in Figure 25(a). From this it can be readily seen that the charge and discharge time constants for the circuit are given by:

$$T_c = R_{DS}(on) \cdot C$$

$$T_d = R_i \cdot C$$

$R_{DS}(on)$ = ON resistance of FET

R_i = input resistance of the following stage

The discharge of the capacitor thru the FET switch is neglected in the OFF position. These equations show the requirement for a good current driver and a high impedance output if a short sampling time and long hold time are desired.

The value of capacitance used is based on a compromise between sample time and hold time and is the only variable in a circuit such as Figure 25(a) since the ON resistance of the FET must be minimized and the input resistance of the next stage maximized for optimum performance.

The two variations of S&H circuits used in construction of the filter are shown in Figure 25(b) and (c) along with their charge and discharge time constants. Some characteristics of the circuits are given below.

Configuration	Flat hold to sample time (max)	Gain	Freq. resp.	Max. input (pk. to pk.)
Potent. 2N3819	40 sec	+1	.9flat	1.5V
Potent. 2N4857	200 sec	+1	.9flat	1.5V
Self-buffered	80 sec	+1	.95flat	1.5V

The self-buffered configuration used a single OPAMP which is time multiplexed for use as both the current driver and the output buffer, and hence requires only a single OPAMP whereas two are required in the Potentiometric configuration. Two N-channel and one P-channel FETs were used as shown in Figure 25(c) so that a single positive pulse could be used to operate the S&H. Reference 11 discusses S&H circuits using FET switches and OPAMPS and provides more information on the general characteristics of the circuits shown in Figure 25.

(a) Basic

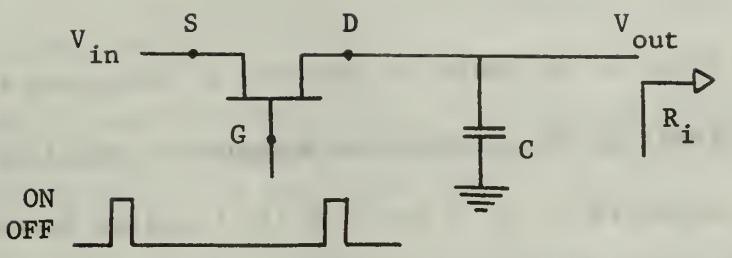

(b) Potentiometric

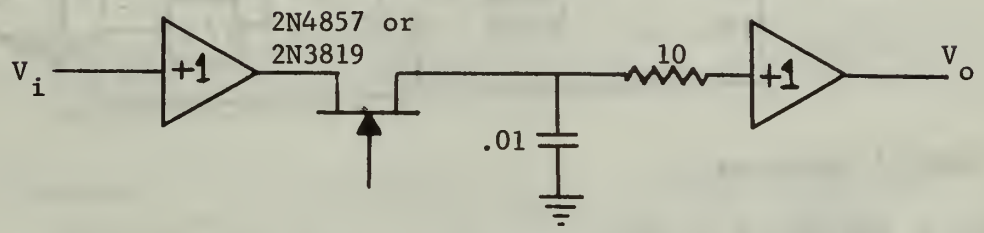

Charging Capacitor

2N3819 Time Constant = 1.6 microseconds
2N4857 Time Constant = 0.4 microseconds

Discharging Capacitor

Both Time Constant = 60 milliseconds

(c) Self-Buffered

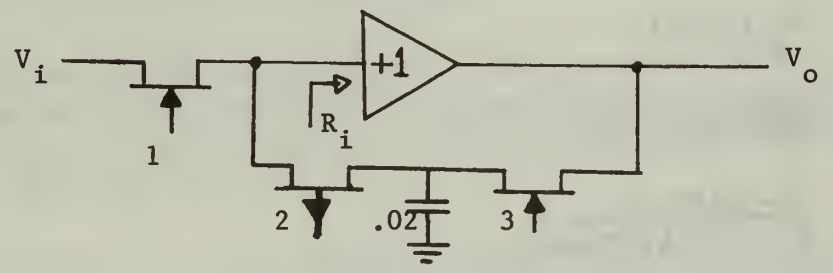

1 and 3-2N3819 Charging Time Constant = 3.2 microsec.
2-2N4360 Discharge Time Constant = 60 millisec.

FIGURE 25: SAMPLE-AND-HOLD CIRCUITS

APPENDIX D

Transfer Function Derivation

In order to calculate the theoretical frequency response given in Table III the equations of Appendix A must be used to find the variables A, B, C and D in the transfer function of the following comb filter (shown in block diagram form).

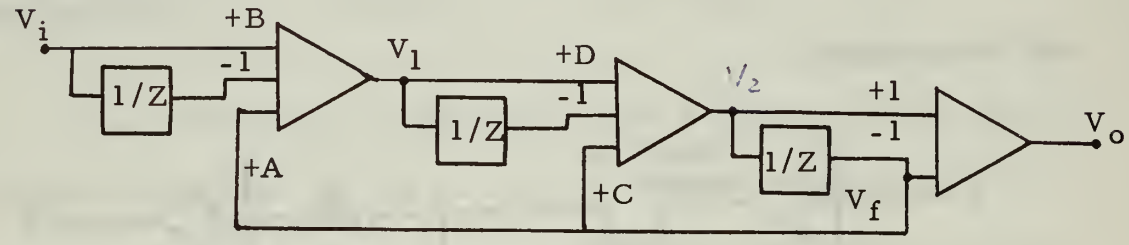

General equations:

$$V_1 = BV_i - V_1/Z + AV_f \qquad V_f = V_2/Z$$

$$V_2 = DV_1 - V_1/Z + CV_f \qquad V_o = V_2 - V_f$$

Solution:

$$V_1 = (B - 1/Z)V_i + (A/Z)V_2$$

$$V_2 = (D - 1/Z)V_1 + (C/Z)V_2$$

$$V_o = V_2(1 - 1/Z)$$

$$V_2 = \frac{DZ - 1}{Z - C} V_1$$

$$V_1 = \frac{(Z-C)(BZ-1)}{Z^2 - (C+AD)Z+A} V_i$$

$$\frac{V_o}{V_i} = \frac{(Z-1)(DZ-1)(BZ-1)}{Z(Z^2-(C+AD)Z+A)}$$

This is the desired transfer function

BIBLIOGRAPHY

1. Skolnik, M. I., Introduction to Radar Systems, McGraw-Hill, New York, 1962.

2. Berg, R. L., and Marshall, P. N., "Integrated Circuits in Action, Part 8: Spotting Targets on the Wing," Electronics, v. 40, p. 58-65, 25 December 1967.

3. Mitchell, L. G., Active Filters with Voltage Variable Pass-band for Application to Range-Gated MTI Systems, Masters Thesis, Naval Postgraduate School, September 1968.

4. Cappadona, W. and Kenneally, D., "A Microminiature MTI System for Surveillance Radars," IEEE Convention Record, p. 34-38, 1966.

5. Zverev, A. I., "Digital MTI Radar Filters," Transactions of IEEE on Audio and Electroacoustics, v. AU-16, No. 3, September, 1968.

6. Nathanson, F. E. and Reilly, J. P., "Clutter Statistics which Affect Radar Performance Analysis," IEEE Supplement to Transactions on Aeronautics and Electronic Systems, November, 1967.

7. White, W. D., "Synthesis of Comb Filters," Proceedings of the National Conference on Aeronautical Electronics, p. 279-285, May, 1958.

8. Linden, D. A. and Steinberg, B. D., "Synthesis of Delay Line Networks," Transactions of IRE Professional Group on Aeronautical and Navigation Electronics, v. ANE-4, No. 1, p. 34-39, March, 1957.

9. White, W. D. and Ruvin, A. E., "Recent Advances in the Synthesis of Comb Filters," Convention Record of the IRE, v. 5, part 2 (Circuit Theory and Information Theory), p. 186-199, 1957.

10. Peterson, R. L., The Synthesis of an MTI Cancellation Filter Using Capacitive Storage Elements in the Delay Line, Masters Thesis, Naval Postgraduate School, June, 1969.

11. Burd, M. and Sears, B., "High Performance Sample and Holds," The Electronic Engineer, v. 26, p. 60-64, December, 1967.

12. Washam, E. L., Synthesis of a Basic Range Channel for Implementation of a Complete MTI by Range-Gated Filtering," Masters Thesis, Naval Postgraduate School, June, 1969.

13. Radio Corporation of America, R. C.A. Linear Integrated Circuits, Electronics Components and Devices Division, Harrison, New Jersey, December, 1967.

14. Fairchild Semiconductor Data Sheet for uA709, 1966.

15. R. C. A. Data Sheet for the CA-3029, January, 1968, file no. 316.

16. Millman, J. M. and Halkias, C. C., Electronic Devices and Circuits, McGraw-Hill, 1967, Chapter 14.

17. Shipley, S. M. Sr., "Analog Switching Circuits Use Field Effect Devices," Electronics, v. 37, p. 45-51, 28 December, 1964.

INITIAL DISTRIBUTION LIST

		No. Copies
1.	Defense Documentation Center Cameron Station Alexandria, Virginia 22314	20
2.	Library, Code 0212 Naval Postgraduate School Monterey, California 93940	2
3.	Professor D. B. Hoisington Department of Electrical Engineering Naval Postgraduate School Monterey, California 93940	1
4.	Captain Harold L. Broberg, USMC 260 Woodland Drive Mount Prospect, Illinois 60056	1
5.	Dr. M. I. Skolnik Director, Radar Division Naval Research Laboratory Washington, D. C. 20390	1
6.	Commandant of the Marine Corps (Code A03C) Headquarters, U. S. Marine Corps Washington, D. C. 20380	1
7.	James Carson Breckinridge Library Marine Corps Development & Educational Command Quantico, Virginia 22134	1

UNCLASSIFIED

Security Classification

DOCUMENT CONTROL DATA - R & D

(Security classification of title, body of abstract and indexing annotation must be entered when the overall report is classified)

. ORIGINATING ACTIVITY *(Corporate author)* Naval Postgraduate School Monterey, California 93940	2a. REPORT SECURITY CLASSIFICATION Unclassified 2b. GROUP

. REPORT TITLE

A Three-Pole Analog Cancellation Filter with Variable Passband for use in Range-Gated Radars

. OESCRIPTIVE NOTES *(Type of report and, inclusive dates)*

Master's Thesis; December 1969

5. AUTHOR(S) *(First name, middle initial, last name)*

Harold Lee Broberg

. REPORT DATE December 1969	7a. TOTAL NO. OF PAGES 78	7b. NO. OF REFS 17
8a. CONTRACT OR GRANT NO. b. PROJECT NO. c. d.	9a. ORIGINATOR'S REPORT NUMBER(S) 9b. OTHER REPORT NO(S) *(Any other numbers that may be assigned this report)*	

10. DISTRIBUTION STATEMENT

This document has been approved for public release and sale; its distribution is unlimited.

11. SUPPLEMENTARY NOTES	12. SPONSORING MILITARY ACTIVITY Naval Postgraduate School Monterey, California 93940

13. ABSTRACT

The design considerations and synthesis procedures involved in construction of a variable-passband analog cancellation filter for use in a range-gated Moving-Target-Indication (MTI) radar are presented. A three-pole Chebychev comb filter built using field-effect transistors and integrated-circuit operational amplifiers was tested and the results are compared with theoretical values. The merits of this type of filter in a range-gated radar are discussed and the performance of a complete range channel containing the filter is compared in the AN/UPS-1 air-search radar with normal radar operation using a delay-line canceller.

DD FORM 1 NOV 65 1473 (PAGE 1)

S/N 0101-807-6811

UNCLASSIFIED

Security Classification

A-31408

14. KEY WORDS	LINK A		LINK B		LINK C	
	ROLE	WT	ROLE	WT	ROLE	WT
Range-Gated Filtering (RGF)						
Range Channel						
Moving Target Indication (MTI)						
Range-Gated Radar						
Pulse Cancellation						
Radar						